Department of Physics
Faculty of Mathematics and Natural Sciences
Technical University Dresden

Domain structure and magnetization processes of complex magnetic multilayers

DISSERTATION

for the partial fulfillment of the requirements for the academic degree of
Doctor rerum naturalium
(Dr.rer.nat.)

by

Dipl.-Phys. **Cristina Bran**

born March 13, 1978 in Slanic-Prahova, Romania

Dresden
2010

Abstract

The magnetization processes of antiferromagnetically (AF) coupled Co/Pt multilayers on extended substrates and of Co/Pd multilayers deposited on arrays of 58 nm spheres are investigated via magnetic force microscopy at room temperature by imaging the domain configuration in magnetic fields.
Adding AF exchange to such perpendicular anisotropy systems changes the typical energy balance that controls magnetic band domain formation, thus resulting in two competing reversal modes for the system. In the ferromagnetic (FM) dominated regime the magnetization forms FM band domains, vertically correlated. By applying a magnetic field, a transition from band to bubble domains is observed.
In the AF-exchange dominated regime, by applying a field or varying the temperature it is possible to alter the magnetic correlation from horizontal (AF state) to vertical (FM state) via the formation of specific multidomain states, called metamagnetic domains. A theoretical model, developed for complex multilayers is applied to the experimentally studied multilayer architecture, showing a good agreement.

Magnetic nanoparticles have attracted considerable interest in recent years due to possible applications in high density data storage technology. Requirements are a well defined and localized magnetic switching behavior and a large thermal stability in zero fields. The thermal stability of $[Co/Pt]_N$ multilayers with different numbers of repeats (N), deposited on nanospheres is studied by magnetic viscosity measurements. The magnetic activation volume, representing the effect of thermal activation on the switching process, is estimated. It is found that the activation volume is much smaller than the volume of the nanosphere and almost independent of the number of bilayers supporting an inhomogeneous magnetization reversal process.

Contents

1 Introduction

The technological requirements of increasing the capability of magnetic recording media and the miniaturization of spintronic devices promote new designs of magnetic structures, such as perpendicular magnetic orientation [Man06], multilayer stacks [Khi06], and patterned nanobits [Ter05].
Multilayer systems with perpendicular magnetic anisotropy are thus attractive since they could be used in multilayer magnetic recording media [Alb05b], spin current-driven magnetic devices [Men06], or magnetoresistive sensors [Din05]. They are expected to improve density, stability, and reliability. At present, the areal densities achieved with longitudinal recording

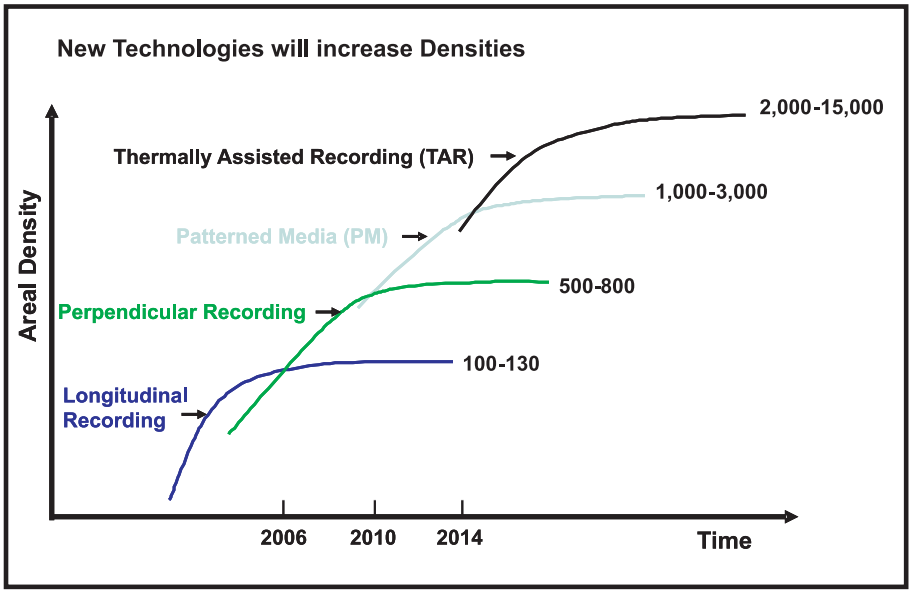

Fig. 1.1: Evolution of areal density in magnetic disk storage, taken from *Hitachi Data Systems*.

media range from 100-150 Gb/in^2 [Fer08]. However the pursuit of higher recording densities is limited by the thermal activation of small ferromagnetic entities known as the "superparamagnetic effect" [Alb05a]. To overcome this problem, perpendicular magnetic recording was introduced recently as an alternative to conventional longitudinal recording [Fer08]. Perpendicular recording has the advantage of achieving higher storage densities and suppressing the superparamagnetic effect by aligning the magnetic recording bits perpendicular to the disk

plate. Therefore, a lot of research work has been carried out on magnetic materials which can be used for the perpendicular magnetic recording. Thus areal densities of 300-400 Gb/in^2 have been achieved. Another approach considered here is bit patterned media. In bit patterned media the aim is to make a single magnetic grain the object of a recording bit, targeting to areal densities beyond 1 Tb/in^2 (Fig. 1.1). Magnetic thin films with strong perpendicular anisotropy, e.g., Co/Pt and Co/Pd multilayers, have been a topic of increasing interest due to their easily tunable magnetic properties and possible applications in perpendicular magnetic recording and patterned media [Koo60, Car85, Hel03, Liu04, Dav04, Rod06, Bar06b]. The magnetization reversal process in these systems usually involves the formation of vertically correlated band domains, i.e. domains of which the magnetization goes through the entire multilayer film stack, resulting from a competition between ferromagnetic (FM) exchange, anisotropy, and dipolar energies [Koo60]. The energy balance can be further tailored by an addition of non-magnetic spacer layers with appropriate thickness, which establishes antiferromagnetic (AF) interlayer exchange coupling [Grü86, Par90, Par91, Bru91, Bru92]. In antiferromagnetically coupled multilayers, both vertically and laterally correlated domain states have been observed. The reversal modes are determined largely by the individual layer thickness and magnetization and by the strength of the AF interlayer coupling. In these samples, $[(\mathrm{Co/Pt})_{X-1}/\mathrm{Co/Ru}]_N$ multilayers, the competition between reversal modes is tuned by N, the number of [Co/Pt] stacks separated by non-magnetic spacer layers, and X, the number of Co layers per [Co/Pt] stack.

The increasing interest in systems with perpendicular anisotropy raises questions on the role of interlayer interactions, both exchange and magnetostatic. Understanding the role of magnetostatic interactions in magnetic layered structures with perpendicular anisotropy is critical for the development of advanced magnetoresistive devices and recording media.

The interlayer exchange coupling has been thoroughly investigated in the past two decades. It was found that the magnetization of two ferromagnetic thin films separated by a nonmagnetic metallic spacer layer is coupled via an exchange interaction mediated by the itinerant electrons of the spacer layer. In this case the interlayer exchange coupling oscillates between ferromagnetic and antiferromagnetic as a function of the nonmagnetic layer thickness [Par90, Par91].
The magnetostatic coupling affects the formation of domains in exchange coupled ferromagnetic multilayers exhibiting perpendicular magnetic anisotropy. For antiferromagnetically exchange-coupled multilayers, this magnetostatic coupling competes with the interlayer exchange interaction resulting in unusual domain structures.

In this context, investigations of the magnetic domain structure are of great interest be-

cause they allow to extract information about magnetization, interactions and anisotropy. Furthermore, a full understanding of the magnetic domain configuration will provide fundamental insights as well as help to achieve technically based objectives, since the magnetization reversal mechanism is closely related to the domain structure.

The aim of this thesis is to study in detail the domain structure and the magnetization processes together with a description of a theoretical model in order to quantitatively describe the complex interactions present in multilayers.

The organization of the thesis is as follows. An overview of existing models describing magnetic domains in thin films and multilayers and some insight into the underlying physics are given in Chapter 2. In Chapter 3 the experimental characterization techniques used in this work are outlined together with some aspects of the sample preparation. In Chapter 4 the experimental results on [Co/Pt]/Ru multilayers with ferromagnetic ground state are grouped. Here, the remanent state is characterized by the above described band domains also common for simple single layer films with perpendicular anisotropy. In-field magnetic force microscopy measurements are performed to follow the evolution of the domain structure in a perpendicular oriented magnetic field in the ascending and descending branches of the first quadrant of the magnetization curve. In the end, the experimental results are compared quantitatively with a modified domain theory for the multilayer architecture investigated in this chapter. Chapter 5 presents the experimental and theoretical data of [Co/Pt]/Ru multilayers with antiferromagnetic ground state. In this case, the AF state transforms into a saturated state via a first order transition accompanied by the formation of multidomain states. In order to investigate field and temperature dependent magnetization reversal, in field domain imaging and magnetic measurements have been performed. Chapter 6 deals with a multilayer system with similar architecture, where the Ru spacer layers are replaced by Ir spacer layers, known for their large mediated AF coupling [Hel07]. The system presents a FM ground state, where the magnetization reversal happens in two distinct steps, showing a new type of magnetization process. Going further towards technological applications, Chapter 7 studies the magnetization reversal of arrays of 58 nm spheres covered by $[Co/Pd]_N$ multilayer stacks exhibiting an out-of-plane magnetization. Such samples are possible candidates for bit-patterned media [Alb05a]. MFM measurements show the individual switching events localized at the sphere locations. The MFM data are correlated with viscosity measurements. The magnetic viscosity is associated with the energy barriers and the activation volume involved in the magnetization reversal and thus allows a better understanding of this process.

2 Fundamentals

2.1 Magnetic domains in films with perpendicular anisotropy

Energy terms

The magnetic domains in thin films display various morphologies. These are determined by many factors such as thickness, strain and applied field and can be understood by a competition of various interactions. Equation (2.1) describes the total energy (disregarding magneto-elastic effects):

$$E_{tot} = \int_V [\underbrace{e_{ex}(m)}_{exchange} + \underbrace{e_{an}(m)}_{anisotropy} - \underbrace{J_s H_{ex}\mathbf{m}}_{ext.field} - \underbrace{\frac{1}{2} J H_d}_{stray field}] dV \tag{2.1}$$

where, $\mathbf{m(r)} = \mathbf{J(r)}/J_s$ is the magnetization unit vector that points in the direction of the local polarization J and J_s is the saturation polarization.

The **exchange interaction** in a ferromagnet favors a parallel alignment of the magnetic moments. Every deviation from this configuration invokes an energy cost which depends on the exchange stiffness constant A [Hub98]:

$$e_{ex} = A[(\nabla m_x)^2 + (\nabla m_y)^2 + (\nabla m_z)^2] \tag{2.2}$$

The **magnetic anisotropy** describes the dependence of the energy on the direction of magnetization. A perpendicular magnetic anisotropy (the easy axis of magnetization is oriented perpendicular to the film surface) can be found in thin films with perovskite-like structure [She59], in orthoferrites [Bob67], or in garnets [Koo60]. In recent years, a perpendicular magnetic anisotropy could also be observed in magnetic multilayers, like: Fe/Pd, Fe/Au, Fe/Gd, Co/Cr, Co/Pd, Co/Pt or Co/Au [Sch99]. The perpendicular anisotropy in multilayers is attributed to the reduced symmetry at the interface between the layers. Other factors like the lattice misfit strain, the interface structure and roughness, atomic mixing

at interfaces, or interfacial magnetocrystalline anisotropy have been considered as a possible additional origin [Cha88, Kyu96].

In the case of uniaxial anisotropy the energy density up to fourth order is given by [Hub98]:

$$e_{an} = K_{u1} sin^2\theta + K_{u2} sin^4\theta \tag{2.3}$$

where θ is the angle between the anisotropy axis and the magnetization direction, and K_{u1} and K_{u2} are material constants. The systems with an easy axis have a large positive K_{u1}, while systems with an easy plane perpendicular to the anisotropy axis have a large negative K_{u1}. Intermediate values, i.e., $-2 < (K_{u1}/K_{u2}) < 0$ describe systems with a "conical" anisotropy.

The **magnetic field energy** can be separated in two terms. The external field term or **Zeeman energy** describes the interaction with an external field, $\mathbf{H}_{ex}$, and depends only on the average magnetization:

$$E_H = -J_s \int \mathbf{H}_{ex} \cdot \mathbf{m} dV \tag{2.4}$$

The second term, the **stray field energy** or **magnetostatic self energy** is related to the demagnetization field, H_d or the magnetic stray field, H_s, generated by the magnetic sample itself [Hub98]:

$$E_d = \frac{1}{2}\mu_0 \int_{outside sample} \mathbf{H}_s^2 dV = -\frac{1}{2} \int_{sample} \mathbf{H}_d \cdot \mathbf{J} dV \tag{2.5}$$

Magnetic domains

Magnetic domains are small areas of the sample that are uniformly magnetized in a given direction. Adjacent domains show a different alignment of the magnetic moments to reduce the total free energy of the system, mainly by reducing the stray field energy.

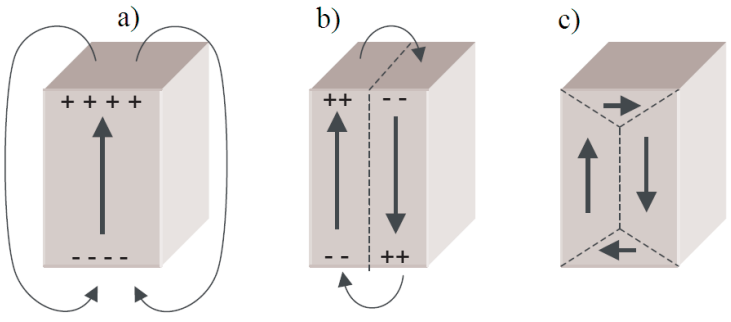

Fig. 2.1: Schematic view of (a) single domain (b) multidomain, (c) closure domain configuration.

Figure 2.1 illustrates the reduction of stray field energy by domain formation. The single domain in Fig. 2.1(a) is assumed to lie parallel to an anisotropy axis and has a large stray field

energy, which is reduced (Fig. 2.1(b)) by the formation of antiparallel domains. At the domain boundaries the magnetic moments are no longer oriented parallel to each other, which leads to an increase in exchange and anisotropy energy. If the material has a cubic anisotropy, or if its uniaxial anisotropy is not too strong, the sample may form closure domains (Fig. 2.1(c)) and thus completely eliminates the stray field contribution. However there is a cost to the formation of these closure domains if the material has a strong magnetostriction (which causes the sample to change shape in the direction of magnetization) or a strong uniaxial anisotropy (which causes the magnetization to align preferentially along the easy axis). Domains are separated by walls, zones in which the magnetization changes its direction in a continuous way. Their dimension is given by the *exchange length*, $l_{ex} = \sqrt{A/K}$, which is determined by the exchange stiffness constant, A and the dominating anisotropy, K. When the shape anisotropy is dominant, the exchange length reads: $l_{ex} = \sqrt{A/K_d}$, with $K_d = J_s^2/2\mu_0$, otherwise it is given by $l_{ex} = \sqrt{A/K_u}$, with K_u being the uniaxial anisotropy constant.

The exchange and anisotropy energies determine the width of domain walls. While the exchange energy favors thin walls, the anisotropy energy is minimized for infinitely extended walls. In thin films the magnetization tends to lie in the plane of the film due to demagnetizing effects of the film shape. In thin films with perpendicular anisotropy the demagnetizing influence is overcome by the uniaxial anisotropy which keeps the moments aligned perpendicular to the film plane. Beside the mentioned energy terms, other parameters, such as the dimension of the sample, external magnetic fields, tension, morphology, or temperature, determine the size of magnetic domains. Consequently, magnetic domains show many different shapes and sizes, reaching from some nanometers to the macroscopic extension of the sample.

2.1.1 Band domains

In the 1960´s Kooy and Enz [Koo60] proposed a model to explain the observed domains in thin films with perpendicular anisotropy. The model assumes parallel bands with alternating magnetization “up” and ”down” (Fig. 2.2). It shows how the formation of magnetic domains is induced by the diminution of stray field energy. The width of the band domains in the absence of an applied field follows from the minimization of wall energy and stray field energy. Kooy and Enz predict the field dependence of band domains in perpendicular magnetic fields by treating the stray field energy in terms of a Fourier expansion and then minimizing the total energy to obtain the magnetization and the equilibrium domain width. The model introduces the expression in the form of two dimensionless parameters: the reduced material

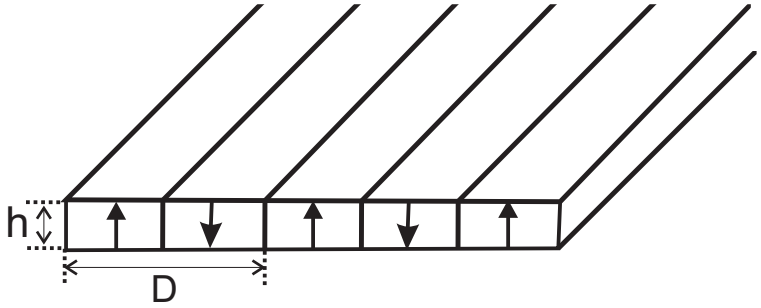

Fig. 2.2: Schematic view of a band domain structure.

anisotropy constant

$$Q = \frac{K_u}{K_d} = \frac{2\mu_0 K_u}{J_s^2} \tag{2.6}$$

which gives the ratio between the anisotropy energy and the demagnetization energy, and the reduced characteristic length:

$$\lambda_c = \frac{e_w}{2K_d h} = \frac{l_c}{h} \tag{2.7}$$

where $e_w = 4\sqrt{AK_u}$ is the domain wall energy. For Q$\gg$ 1, the stray field energy is given as:

$$E_d = K_d h \left\{ m^2 + \frac{4p}{\pi^3} \sum_{n=1}^{\infty} n^{-3} \sin^2[\frac{\pi}{2} n(1+m)][1 + \exp(\frac{-2\pi n}{p})] \right\} \tag{2.8}$$

with d_1, d_2 = domain widths

D=d_1+d_2 = domain period

h= film thickness

$m = (d_1 - d_2)/(d_1 + d_2)$ = reduced magnetization

$p = (d_1 + d_2)/h$ = reduced period

By adding wall energy and Zeeman energy to the stray field energy, the total energy is minimized with respect to p and m, and yields:

$$\lambda_c = \frac{p^2}{\pi^3} \sum_{n=1}^{\infty} n^{-3} \left[1 - (1 + 2\pi n/p) \exp(-2\pi n/p)\right] \cdot \sin^2 \left[\frac{\pi}{2} n(1+m)\right] \tag{2.9}$$

$$h^* = m + \frac{p}{\pi^2} \sum_{n=1}^{\infty} n^{-2} \sin\left[n\pi(1+m)\right] \left[1 - \exp(-2\pi n/p)\right] \tag{2.10}$$

These are two equations that yield, for every pair of reduced period p and of reduced magnetization, the corresponding values of the reduced characteristic length λ_c and the reduced bias field h^*.

Figure 2.3 (a) shows magnetization curves calculated for different values of λ_c. The domain

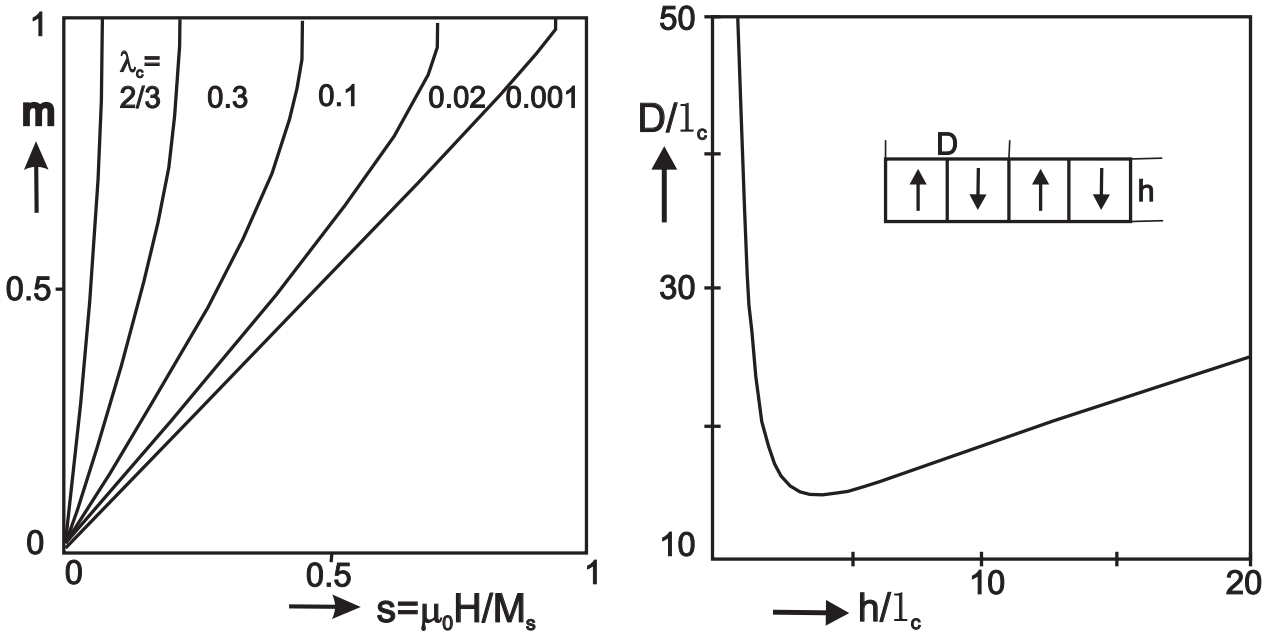

Fig. 2.3: Equilibrium magnetization curves of band domains as a function of a perpendicular applied magnetic field (a) and the equilibrium band domain period D=d_1+d_2 as a function of the film thickness in zero field (b).

wall energy (expressed as a function of λ_c) has little influence on the magnetization curve for small λ_c (large thicknesses) [Hub98]. With increasing λ_c (small thicknesses) the initial slope of magnetization increases and saturation is reached in fields smaller than the demagnetizing field. Figure 2.3 (b) shows the domain period D at zero field in function of the material characteristic length l_c. For small thicknesses ($h < l_c$), the sample forms huge domains. The domain width decreases by reducing the film thickness to a critical value of $4l_c$. For $h > 4l_c$ the domain width increases again.

2.1.2 Bubble domains in thin films

Magnetic bubbles are cylindrical domains of reversed magnetization in a thin film. Magnetic bubbles can exist in materials with $Q = 2K_u/\mu_0 M_s^2 > 1$ and in the presence of an external applied magnetic field [Esc81]. Even when $Q > 1$ and the magnetization is oriented perpendicular to the film it is favorable for the magnetization to break up into a band domain structure to minimize the total energy. By applying a field, the band domain structure (Fig. 2.4(a)) transforms into isolated bubbles (Fig. 2.4(b)). The isolated bubbles require an external magnetic field, H in order to be stable. If H is reduced, the isolated bubbles transform into isolated stripe domains in order to increase the volume fraction of the minority domain and thus reduce Zeeman energy. The field at which this occurs is called *strip-out field* (H_{bs}).

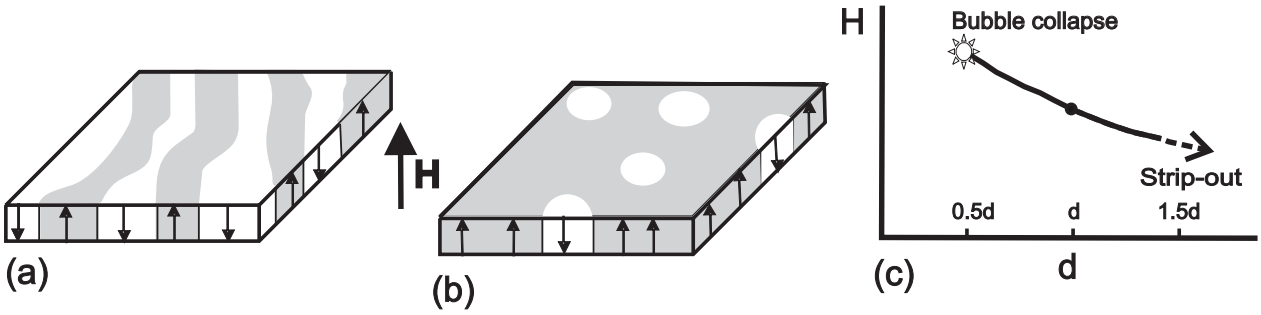

Fig. 2.4: Schematic view of (a) a band domain structure, (b) bubble domains and (c) evolution of bubbles in magnetic field.

If H is increased, the magnetic orientation of the volume outside of the bubbles becomes more favorable and above a critical field, *collapse field* H_{bc}, the bubbles collapse. The bubble size varies in a field range limited by the two critical fields, strip-out and collapse field (Fig. 2.4(c)). The deviation from the equilibrium configuration of an isolated bubble was calculated by Thiele [Thi70]. It was assumed that the equilibrium configuration is circular and the instability occurs when the applied field is reduced to the critical value of the strip-out field. Figure 2.5 shows the domain model considered. The single cylindrical domain exists in

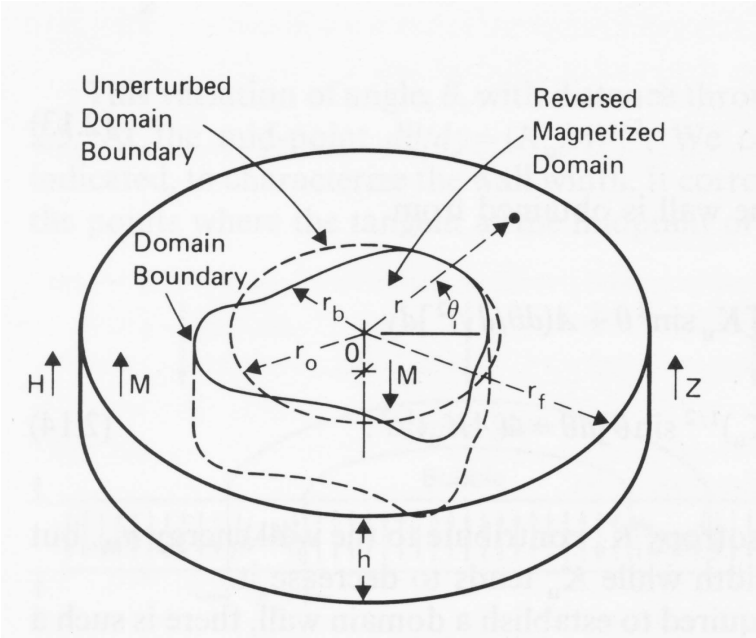

Fig. 2.5: Schematic view of the domain configuration.

a plate with perpendicular anisotropy and thickness h. The domain wall is assumed to have negligible width and to be characterized by a wall energy density σ_w, which is independent of the wall orientation or curvature.

The domain shape is described by the expansion:

$$r_b(\theta) = r_0 + \Delta r_0 + \sum_{n=1}^{\infty} \Delta r_n \cos[n(\theta - \theta_n - \Delta\theta_n)] \tag{2.11}$$

where Δr_n and $\Delta\theta_n$ describe the variation from a circular domain, and θ_n gives the direction of variation. The circular domain has a radius that differs from the radius of a circular bubble, r_0, by an amount Δr_0. Domain size and stability are characterized by the first and second derivative of the total energy E_T with respect to Δr_n and $\Delta\theta_n$.

$$\begin{aligned} \Delta E_T &= \sum_{n=0}^{\infty} \left[\left(\frac{\partial E_T}{\partial r_n} \right)_0 \Delta r_n + \left(\frac{\partial E_T}{\partial \theta_n} \right)_0 \Delta\theta_n \right] \\ &+ \frac{1}{2} \sum_{n=0}^{\infty} \sum_{m=0}^{\infty} \left[\left(\frac{\partial^2 E_T}{\partial r_n \partial r_m} \right)_0 \Delta r_n \Delta r_m + 2 \left(\frac{\partial^2 E_T}{\partial r_n \partial \theta_m} \right)_0 \Delta r_n \Delta\theta_m + \left(\frac{\partial^2 E_T}{\partial \theta_n \partial \theta_m} \right)_0 \Delta\theta_n \Delta\theta_m \right] \\ &+ 0_3 \end{aligned} \tag{2.12}$$

In Eq. (2.12) zero subscripts represent the evaluation of the derivative when the domain is circular and 0_3 refers to the terms of order three and higher in the combination of Δr_n and $\Delta\theta_n$ [Thi69].
Here, many of the terms are zero $\left(\frac{\partial E_T}{\partial r_n}\right)_0$, $\left(\frac{\partial E_T}{\partial \theta_n}\right)_0$ but not $\left(\frac{\partial E_T}{\partial r_0}\right)_0$ [Thi69]. Thus, the system is in equilibrium for

$$\left(\frac{\partial E_T}{\partial r_0} \right)_0 = 0 \tag{2.13}$$

which represents the first derivative of the total energy , the so-called *force function*. For the system to be stable, the second derivative should be positive: $\left(\frac{\partial^2 E_T}{\partial r_n^2}\right)_0 > 0$. Normalizing the total energy to the magnetic energy of a volume $2\pi h^3$ containing an uniform magnetic field of magnitude J_s/μ_0, yields:

$$\begin{aligned} \frac{\Delta E_T}{J_s^2} \frac{2\mu_0}{\pi h^3} &= \left[\frac{l_c}{h} + \frac{\mu H}{J_s} - F\left(\frac{d}{h}\right) \right] \frac{\Delta r_0}{h} \\ &- \left[\frac{l_c}{h} - S_0\left(\frac{d}{h}\right) \right] \frac{d}{h} \left(\frac{\Delta r_0}{h} \right)^2 \\ &+ \frac{1}{2} \sum_{n=2}^{\infty} \left(n^2 - 1\right) \left[\frac{l_c}{h} - S_n\left(\frac{d}{h}\right) \right] \frac{h}{d} \left(\frac{\Delta r_n}{h} \right)^2 + 0_3 \end{aligned} \tag{2.14}$$

where F and S_n are defined as a *force* and a *stability function*, respectively and are functions of complete elliptic integrals of the first and second order [Thi69]. The equilibrium diameter of the bubble is obtained from the first order variation, which yields:

$$\frac{l_c}{h} + \frac{\mu_0 H}{J_s}\frac{d}{h} - F\left(\frac{d}{h}\right) = 0 \tag{2.15}$$

Equation (2.15) is displayed graphically in Figure 2.6. The values of l_c and $\mu_0 H/J_s$ define

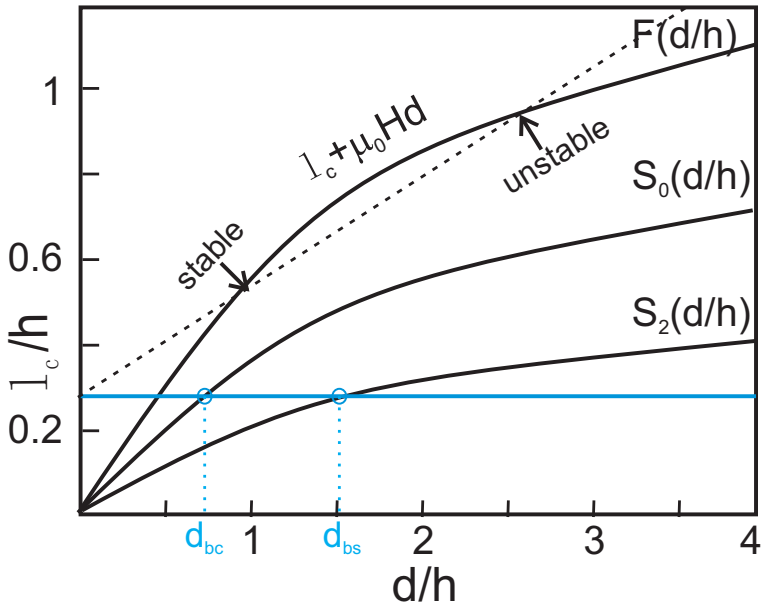

Fig. 2.6: The force and stability functions versus bubble diameters.

a straight line which intersects the force curve $F(d/h)$ twice. The diameters at which this intersection occurs are the solutions of Eq. (2.16). However, these solutions can be stable or unstable. The stability criteria come from the second order variation and are:

$$\frac{l_c}{h} - S_0\left(\frac{d}{h}\right) < 0 \tag{2.16}$$

and

$$\frac{l_c}{h} - S_n\left(\frac{d}{h}\right) > 0,\ n \geq 2 \tag{2.17}$$

These two functions are plotted also in Figure 2.6. Using the plot and $l_c/h = S_0(d_{bc}/h) = S_2(d_{bs}/h)$, the critical diameters, d_{bc} and d_{bs}, are obtained. Together with Eq. (2.16) also the critical fields, H_{bc} and H_{bs}, are determined. In the field range between these two critical fields the magnetic bubbles are stable.

2.2 Magnetic multilayers

Magnetic multilayers formed by a repeated stack of a magnetic metal (such as Fe, Co or Ni) alternating with a non-magnetic metal (such as Cu, Pd or Pt) were investigated for possible applications as magneto-optical recording media [Zep89, Lin92] and to study low dimensional magnetic phenomena. The result of this work was the discovery of perpendicular magnetism [Gra77, Car85, Car88] and enhanced magneto-optical effects in novel layered materials, of oscillatory exchange coupling as a function of the thickness of a layer of spacer materials separating two magnetic films [Maj86] and of giant magnetoresistance (GMR) in similar layered materials [Grü86, Bai88].

2.2.1 Interface anisotropy

Two important reasons for magnetic anisotropy are the dipolar interaction and the spin orbit interaction. The dipolar interaction depends on the shape of the specimen and is responsible for the in-plane magnetization usually observed in thin films. Locally, the spins are coupled via the spin-orbit interaction to the orbits, which are influenced by the crystal lattice. In this case, the spin-orbit interaction induces a small orbital momentum, which couples the total magnetic moment to the crystal axes [Joh96]. This results in a total energy which depends on the orientation of the magnetization relative to the crystalline axes and reflects the symmetry of the crystal.

As the individual layers in the magnetic multilayers have a thickness of just a few atomic layers, the role of surfaces and interfaces may dominate that of bulk; this is the case for various magnetic multilayers where a perpendicular interface contribution to the magnetic anisotropy is capable of rotating the easy magnetization direction from in the film plane to an orientation perpendicular to the film plane. For the first time this type of anisotropy was predicted by Néel [Née54] and results from the lower symmetry at surfaces or interfaces.
Experimentally, perpendicular magnetic anisotropy was observed in multilayers by Carcia et al. [Car85, Car88] in Co/Pd and Co/Pt, respectively, and later in other Co-based multilayers, such as Co/Au [dB88], Co/Ru [Oun92] and Co/Ir [dB91].
In all these studies the magnetic anisotropy energy K (defined per unit volume) is separated into a volume contribution, K_v, and an interface contribution, K_s, and is sometimes indicated as effective anisotropy, K_{eff}:

$$K = K_{eff} = \frac{2K_s}{h} + K_v \tag{2.18}$$

A positive K describes the case of a perpendicular magnetization. The equation represents

the average of the magnetic anisotropy energy of the interface atoms and the internal atoms of a magnetic layer of thickness h. The factor 2 comes from the two interfaces of each Co layer. The volume anisotropy, K_v includes the magnetostatic or demagnetizing energy and the magnetocrystalline anisotropy. The determination of K_v and K_s can be obtained by a plot of the product Kh versus h.

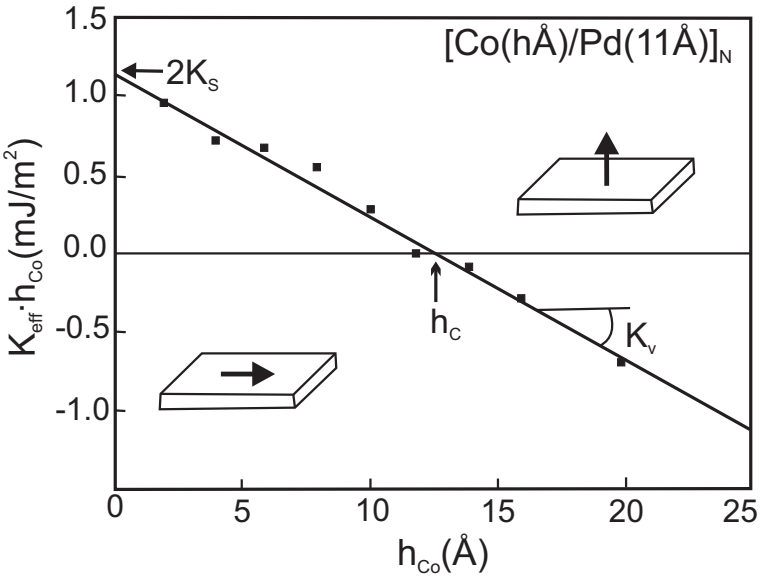

Fig. 2.7: Magnetic anisotropy energy versus the individual layer thickness of Co/Pd multilayers [dB91].

Figure 2.7 shows a typical example of such a plot for Co/Pd multilayers [dB91]. The negative slope indicates a negative volume anisotropy, K_v, favoring an in-plane magnetization due to the dominating shape anisotropy. Up to a critical thickness $h_c = -2K_s/K_v$ the interface anisotropy contribution exceeds the volume contribution, resulting in a perpendicular effective anisotropy. Experimentally, many factors such as roughness or formation of interface alloys may cause a variation in perpendicular magnetic anisotropy. The effect of roughness on the anisotropy was studied theoretically by Bruno [Bru88]. A rough surface can be characterized by an average fluctuation amplitude σ, which is the mean square deviation from the ideally flat surface, and the correlation length ξ, the average lateral size of flat areas on the surface (terraces and craters). Roughness creates in-plane demagnetizing fields at the edges of terraces, thereby reducing the shape anisotropy. The anisotropy contribution resulting from the roughness will, therefore, always be positive (favoring perpendicular magnetic anisotropy) [Bla94].

Interdiffusion might occur during the deposition of multilayers. Draaisma et al. [Dra88] showed that when the layers are interdiffused, K_s has a strong dependence on the degree of mixing.

In addition, it was shown that the effective perpendicular magnetic anisotropy also depends on the crystal orientation in Co-based multilayers. For instance, the (111) orientation favors the perpendicular anisotropy in Co/Pt multilayers compared to (100) or (110) growth orientations [Lee90, Lin92, Can87].

2.2.2 Antiferromagnetic coupling

Coupled magnetic layers have attracted a lot of interest in the last decade because of the discovery of two interesting effects in ferromagnetic transition metal films separated by non-magnetic layers. The first effect is that the ferromagnetic layers can couple antiparallel to each other and form an antiferromagnetic (AF) system [Grü86]. The second effect is that an AF coupled system can exhibit a giant magnetoresistance effect (GMR) [Bai88]. The magnetic coupling in these complex multilayers oscillates between ferromagnetic and antiferromagnetic as a function of spacer layer thickness [Par90].

Various architectures of materials, in sandwiches or multilayers, have been examined in terms of their coupling and the oscillation period [Hei94]. In multilayers, the oscillation periods are between 8-12 Å for almost every metal spacer layer and no multiperiodicity was observed [Par90]. Multiperiodicities, that imply both short (about 2 monolayers) and long-range (about 5-6 monolayers) periodicities of interlayer coupling have been reported in few well controlled sandwich systems. However, in multilayer systems, short range coupling oscillations have not been observed so far, despite theoretical predictions, probably due to the roughness at the interface [Bru91, Bru92].

Oscillatory coupling between Co layers across a Ru spacer layer was first investigated by Parkin et al. [Par90]. Figure 2.8 shows the dependence of the saturation field on the thickness of the Ru spacer layer for Ru(100 Å)/[Co(20 Å)/Ru(t)]$_{20}$/Ru(50 Å) multilayers, deposited at different temperatures. The saturation field can be displayed in terms of the strength of the antiferromagnetic coupling as $-4J_i = H_s M h_{FM}$ [Par90] where M and h_{FM} are the magnetization and the thickness of the ferromagnetic layer, respectively. The saturation field H_s increases as the Ru layer thickness decreases below 8 Å. As the Ru thickness is increased, the saturation field decreases to small values in the range of 10-14 Å. As the Ru thickness is increased further, H_s reaches a maximum at $\simeq$18 Å and a second one at $\simeq$31 Å. The data show that the strength of antiferromagnetic coupling is related to the Ru thickness and oscillates with a period of $\simeq$ 12-14 Å.

Generally, the AF coupling in these systems can result from the combination of two contributions [Sti93]:

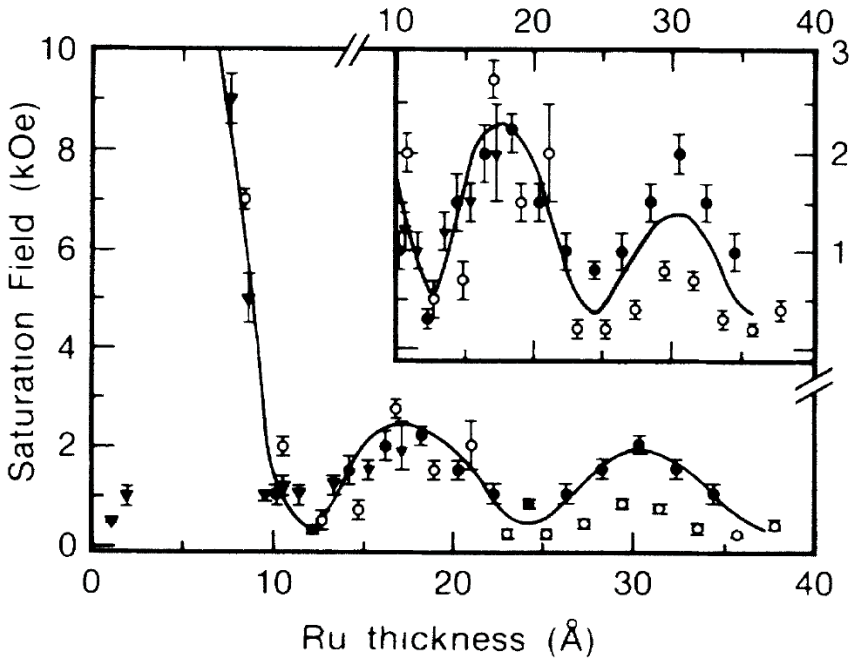

Fig. 2.8: Saturation field vs Ru layer thickness for Co/Ru multilayers deposited at 40°C (solid symbols) and 125°C (open symbols) [Par90].

- The exchange coupling mediated by the conduction electrons, which oscillates as a function of the metallic spacer thickness and which suggests the involvement of the Ruderman-Kittel-Kasuya-Yosida (RKKY) theory.
- The dipolar magnetic coupling, known also as Néel coupling or "orange-peel" coupling, which comes from the magnetostatic charges at the interfaces and is induced by surface roughness.

Oscillatory exchange coupling (RKKY-type): In systems formed by ferromagnetic layers separated by non-magnetic spacer layers, the magnetization of each ferromagnetic layer is coupled with the next ferromagnetic layer through the electrons of the spacer layer. The RKKY interaction [Rud54, Yos57] is long ranging and oscillatory and was used to describe the indirect coupling of both electronic and nuclear magnetic moments by conduction electrons [Hei94].

However, one must consider the itinerant nature of electrons in transition metal ferromagnets which gives rise to the spin-split band structure and spin-dependent reflectivities at the non-magnetic/ferromagnetic interfaces. The spin-dependent reflectivity is illustrated in Fig. 2.9, where it is assumed that electrons with their spins parallel (antiparallel) to the magnetizations M_1 and M_2 are weakly (strongly) reflected at these interfaces. Spin up ($\uparrow$) electrons can penetrate the whole stack with little reflection at the interfaces. For spin down ($\downarrow$) electrons, due to the splitting of the bands in the magnetic films, the transmission of electrons

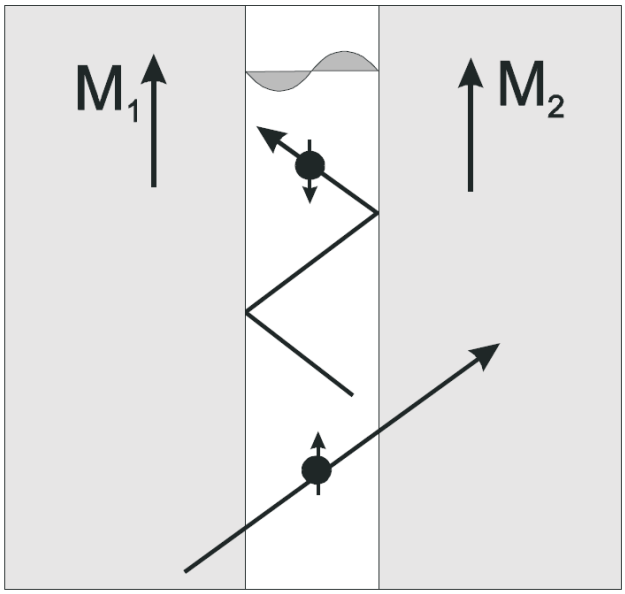

Fig. 2.9: Spin-down electron reflected back and forth between the interfaces and spin-up electron, which can penetrate the whole stack with little reflection at the interfaces.

is reduced leading to a stronger confinement. With respect to the motion of the electrons perpendicular to the interfaces a spectrum of discrete energy levels is obtained corresponding to the formation of standing electron waves. When the interlayer thickness is increased, the discrete levels shift downwards and new levels come in and are populated upon crossing the Fermi energy (E_F). The result is an increase of the electronic energy when such a level just crosses E_F. To lower its energy the system changes the magnetization direction from parallel to antiparallel alignment. For discrete levels far below E_F, with low energy, a parallel alignment of magnetization directions will be more favorable. Therefore, upon increasing the spacer thickness, an oscillatory magnetic coupling is expected. The stronger the confinement and the higher the changes in the density of states, the larger will be the associated coupling amplitudes.
For an antiferromagnetic alignment of the magnetic films, both up and down spins are less confined and no standing waves are formed. Taking into account the real band structure of all three layers, the exchange coupling between ferromagnetic layers separated by nonmagnetic spacer layers is a product of the electronic and geometrical properties of the Fermi surface of the spacer layer material and the reflection amplitudes from the interfaces [Sti93].

Magnetostatic (orange-peel) coupling: Néel studied the magnetostatic coupling between two ferromagnetic layers due to the magnetic dipoles at the interfaces induced by the roughness of layers [Née62]. This so called *orange-peel coupling* is ferromagnetic when the adjacent inter-

faces present the same correlated in-phase waviness and decreases exponentially with spacer layer thickness. Moritz et al. [Mor04] extended Néel's theory of magnetostatic coupling to the case of multilayers with perpendicular anisotropy and showed that the presence of roughness at the interfaces induces an interlayer coupling that can favor either parallel or antiparallel alignment of the magnetization between two ferromagnetic (FM) layers.

Two FM layers, F_1 and F_2, of thickness t are separated by a non-magnetic spacer layer (NM)

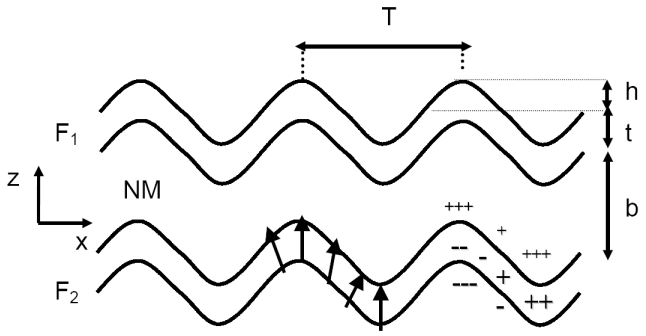

Fig. 2.10: Schematic of layer geometry, consisting of two FM layers, F_1 and F_2, separated by a non-magnetic spacer layer, NM [Mor04].

of thickness b (Fig. 2.10). The roughness of the FM layers is assumed to be correlated (in-phase) where h and T are the amplitude and the wavelength of the roughness, respectively. It is assumed that the dominant anisotropy term is the interfacial anisotropy and that the local anisotropy axis always points along the normal to the interface. Due to the perpendicular anisotropy, the magnetization is in average perpendicular to the plane (Fig. 2.10). However, due to the misalignment of the anisotropy axes caused by the interfacial waviness, the magnetization oscillates spatially. The total energy of the system is a sum of the anisotropy, exchange and magnetostatic energies.

It was found that magnetostatic coupling ("orange-peel") can favor either parallel or antiparallel alignment with out-of-plane anisotropy depending on the relative amplitude of the exchange stiffness constant and the magnetic anisotropy. For low values of the anisotropy constant, the coupling favors a parallel alignment of the magnetization. In this case the magnetization remains uniformly perpendicular to the plane, as illustrated in Fig. 2.11(a), in order to minimize the surface charges and because of the exchange stiffness. In this case, there are no volume charges because the magnetization is almost uniform within each layer. It results that the main magnetostatic interaction is the interaction between the charge densities which are facing each other at the F_1/NM and NM/F_2 interfaces. Since these charges

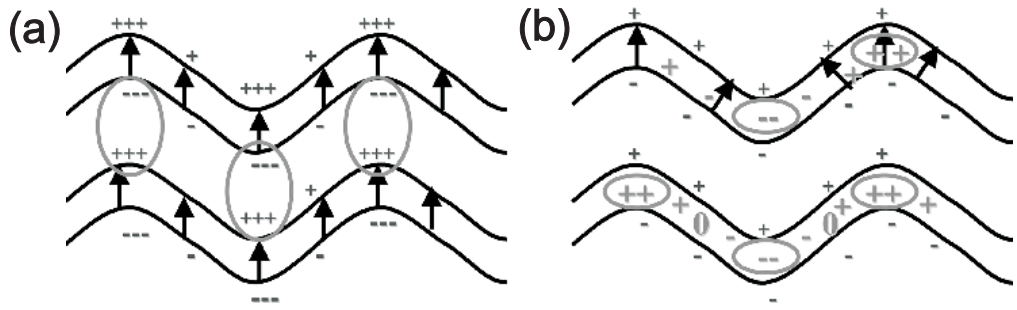

Fig. 2.11: (a) Illustration of the magnetization in the case of low anisotropy. The average magnetization being parallel to the z-axis, magnetic charges of opposite signs appear on the interfaces generating a parallel coupling. (b) For large anisotropy, the magnetization follows the normal to the surface. The volume charges of the same sign in the magnetic layers generate an antiparallel coupling. [Mor04].

are opposite in the parallel magnetic configuration, the parallel alignment is favored in this case.

When the anisotropy is large, the magnetization follows the normal to the interface as shown in Fig. 2.11(b). Here, the interfaces are uniformly charged and generate no coupling. But a large oscillatory distribution of volume charges arises due to the divergence of the magnetization in the x-direction. For a parallel magnetic alignment, the volume charges oscillate in phase in F1 and F2 which is unfavorable from a magnetostatic point of view since charges of the same sign are facing each other. Consequently, this situation favors an antiparallel alignment of the magnetization.

2.3 Review of domain studies on AF coupled multilayers

Due to the progress made in the development of new and good techniques for high-quality thin film deposition, the surface and interface determined properties of magnetic materials attracted much interest. The discovery of the GMR effect [Grü86, Bai88] and the interlayer exchange coupling [Maj86, Par90] in magnetic multilayers consisting of thin ferromagnetic layers spaced by non-magnetic layers have led to intense theoretical and experimental studies in the past years.
Parkin et al. [Par90] observed that antiferromagnetic (AF) coupling across non-magnetic layers is an oscillatory function of the interlayer thickness and changes from FM to AF and vice versa. An oscillatory coupling was observed in Co-based multilayers with 3d, 4d and 5d transition metal spacer layers, with an oscillation period of about 5-6 monolayers and different coupling strength as function of the spacer thickness. Interlayer exchange coupling has been observed experimentally for a wide variety of spacer materials such as nonmagnetic metals (Ru, Cu, Au, etc.) [Par90,Par91] and AF metals (Cr, Mn) [Grü86,Bai88,Ung91] or insulating (MgO and NiO) and semiconducting (Si, Ge) materials [Liu03, Liu04, FV02, Pop02].
So far almost all investigations were carried out on layered magnetic thin films with in plane magnetization. Recently, Co/Pt or Co/Pd multilayers were used as FM layers for their perpendicular anisotropy, attracting considerable attention due to their possible application in perpendicular magnetic storage technology.

The so far best studied system is $[(Co/Pt)_{X-1}/Co/Ru]_N$ [Hel03, Hel07], which is formed by individual Co/Pt stacks, separated by thin Ru spacer layers (Fig. 2.12(a)). This produces a competition between magnetostatic coupling and AF exchange coupling. The perpendicular anisotropy of the Co/Pt system originates from the Co surface anisotropy and can be tuned via the individual Co layer thickness, while the total magnetic moment can be varied independently via the number of Co/Pt repeats and the ratio of the Co and Pt layer thicknesses. The Co layers are strongly ferromagnetically coupled across the Pt layers and each separate Co/Pt stack can be seen as a single FM layer (see Section 2.2.1). Layering Co/Pt multilayers separated by Ru spacer layers introduces an AF exchange coupling between adjacent Co/Pt stacks whose strength is tuned via the Ru thickness [Hel03].
Figure 2.12(b) indicates the remanent domain state of the [Co/Pt]/Ru system as function of the sample architecture. It is distinguished between a so-called AF state, where the magnetization is laterally correlated in each individual Co/Pt stack but antiparallel from stack to stack and the FM ground state where the magnetization is correlated in vertical direction forming band domains. For small X (the number of Co/Pt repeats per block) and small N

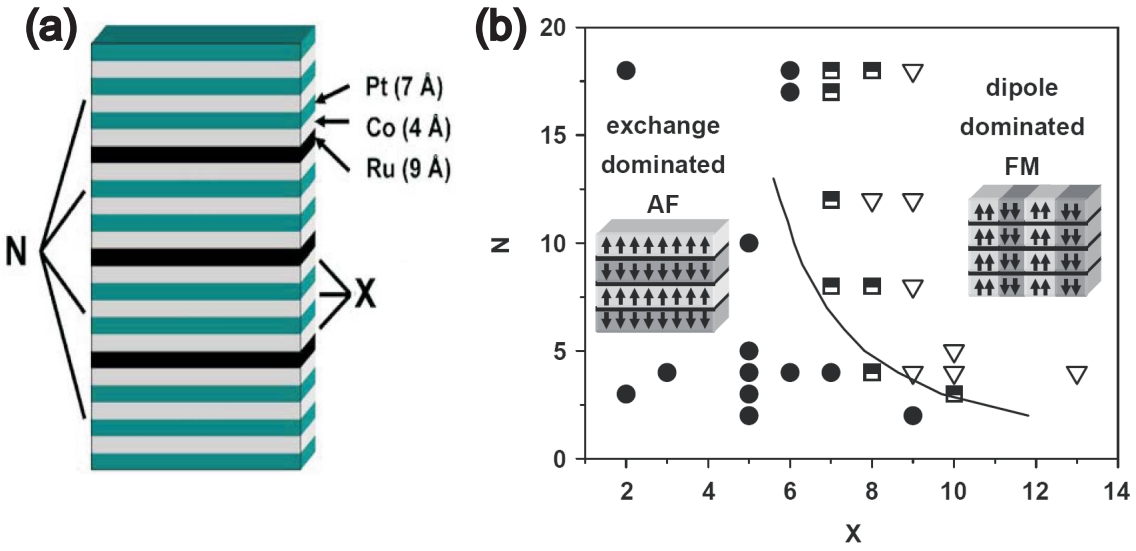

Fig. 2.12: (a) Schematic illustration of the multilayer structure (b) Phase diagram of the magnetic ground state configuration in $[(Co/Pt)_{X-1}/Co/Ru]_N$ multilayers depending on N and X. AF-coupled ground states are shown in solid circles, while FM states are shown in open triangles. The mixed state is marked by half filled squares [Hel07].

the system displays an AF ground state, while for large X or N the system prefers the FM ground state (with a characteristic band domain structure (Chapter 4)). In between, there is a transition region, where the system displays a mixed state that results in a ground state which depends on the magnetic history (Chapter 5). Figure 2.13 displays the MFM remanent states of $[(Co/Pt)_{X-1}/Co/Ru]_N$ thin films for the case N=4, after in-plane and out-of-plane saturation, respectively. Below the transition from AF to FM (X<8), the system displays micrometer AF domains after in-plane saturation and a uniform AF state after out-of-plane saturation. At the transition (X=8) the system reveals a mixed behavior. After in-plane saturation the sample shows FM domains but develops an uniform AF state after out-of-plane saturation. For X>8, the FM magnetic domains develop independent of the magnetic history [Hel07] (for more details see Chapters 4 and 5).

Whereas the remanent domain state in this system is well characterized (Fig. 2.12) and understood in the framework of a simplified domain theory ignoring the details of the layered structure, the magnetization processes and the rich variety of the domain configuration in an external field are not well studied. They present the topic of Chapters 4 and 5 in this thesis. Another study addressed the Néel-type magnetostatic coupling through the correlated roughness of a metallic spacer layer, as described in Section 2.2.2.

The developed theoretical model [Mor04] was applied to $[Pt(2\ nm)/Co\ (0.4\ nm)]_4/Pt(t_{Pt})/[(Co\ (0.4\ nm)/Pt(2\ nm)]_3/(Co\ (0.4\ nm)/PtMn(7.5\ nm)$. The coupling was found to be parallel for all Pt thicknesses and rapidly decreases as the thickness increases. The decrease was

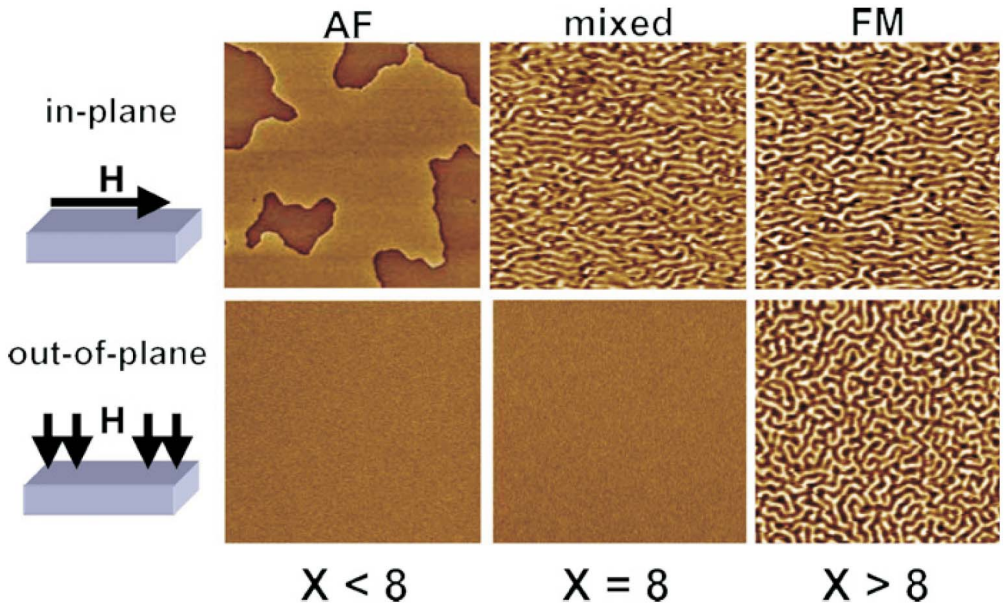

Fig. 2.13: MFM images ($5\mu m^2$ $\times 5$ μm^2) recorded after in-plane (top) and out-of-plane saturation (bottom) for AF-coupled Co/Pt/Ru systems with X=5, 8 and 13 [Hel07].

found to be non-monotonous and an oscillatory behavior was found with a local maximum in the coupling amplitude around 3.8 and 5 nm [Mor04]. It was observed that in the range of thickness corresponding to the local minimum of interlayer coupling ($\approx$ 3.5 nm), the ground state of the system is antiferromagnetic. In contrast, around a Pt thickness of 3.8 nm, the initial magnetization was equal to the saturation magnetization indicating a ferromagnetic coupling [Mor04].

Baltz et al. [Bal07] studied the domain replication resulting from interlayer magnetostatic coupling in trilayers formed by two $(Co/Pt)_X$ layers separated by a thick Pt layer. Samples consisting of stacks of two ferromagnetic multilayers (soft and hard layer) separated by a thick non-magnetic spacer layer $(Co/Pt)_2/Pt_X/(Co/Pt)_4$ with perpendicular magnetic anisotropy have been DC sputtered on a continuous silicon substrate. The spacer thickness, x, varies from 4 to 100 nm. As in the previous examples, each Co/Pt stack can be considered as a single ferromagnetic layer. The effects resulting from magnetostatic interaction on the domain configuration for different Pt spacer layer thicknesses were investigated by MFM. For a thin Pt spacer thickness, the stray field of the bottom layer combines with that from the top layer. The images displayed only bright and dark contrast. The absence of the "gray" (intermediate) contrast results from the domain replication due to the strong interlayer magnetostatic interactions [Rod06]. For thick Pt spacer thicknesses, the stray field from the bottom layer becomes too weak and only the stray field coming from the top layer is probed.

Recently, oscillatory interlayer coupling was observed in *(Co/Pt)/NiO/(Co/Pt)* multilayers with out-of-plane anisotropy [Liu03, Liu04, Bar06a, Bar06b]. The interlayer coupling oscillates

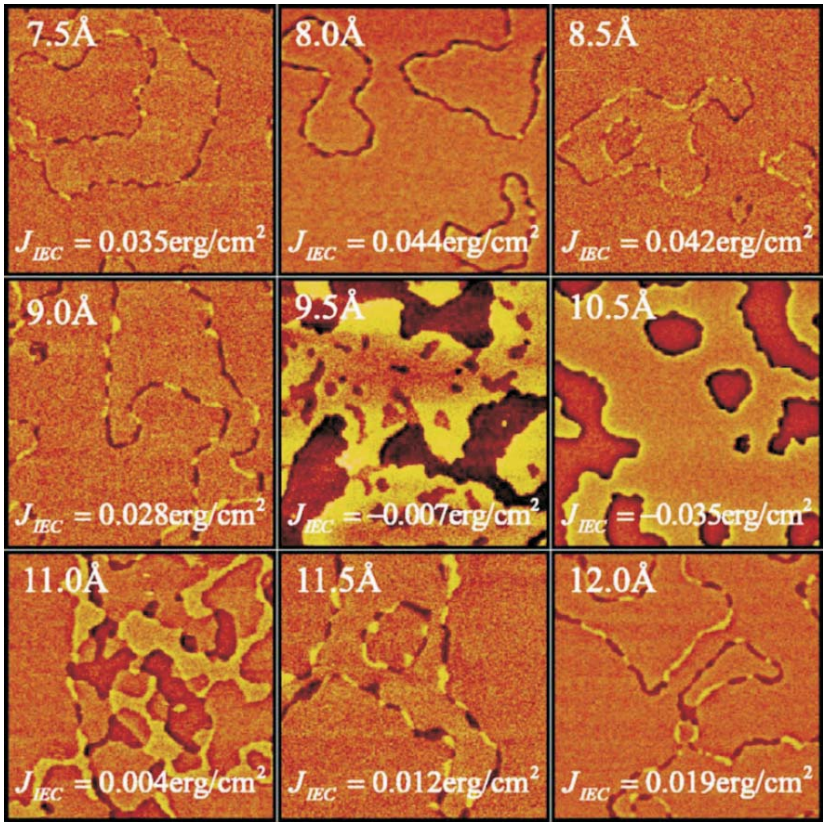

Fig. 2.14: MFM images ($5\mu m^2$ $\times 5$ μm^2) of coupled Co/Pt multilayers with different thicknesses of the NiO spacer layer [Bar06a].

between FM and AF as a function of NiO spacer thickness with a period of $\sim$ 5 Å or 2 monolayers [Liu04]. Figure 2.14 shows MFM images of AF coupled [Co(0.4 nm)/Pt(0.6 nm)]/NiO(t_{NiO})/[(Co(0.4 nm/)Pt(0.6 nm)] for different NiO thicknesses [Bar06a]. The coupling strength, J, varies with the NiO thickness as is indicated on the individual figure panels. The positive (negative) value of J corresponds to AF(FM) coupling. In FM-coupled samples, the domains are coupled vertically through the whole stack leading to a net up-down configuration. In AF coupled samples, the magnetization is only laterally correlated leading to a zero net magnetization. Here, the magnetic contrast arises from the regions where magnetization changes from "up" to "down". It was shown that there is a lateral shift between the domains in the upper and lower Co/Pt layers. The domain wall possesses a net magnetic moment and is wider (>130 nm) than the expected domain width in these films (14-22 nm). The overlap region varies in width with the strength of AF coupling [Bar06b]. The same behavior was observed in the case of Co/Pt multilayers separated by Ru or Pt.

AF interlayer coupling through an insulating spacer was evidenced also in the case of

Fe/MgO/Fe/Co [FV02]. The AF coupling is observed for t_{MgO}<0.8 nm, with a very fast increase of amplitude when the thickness of the spacer is reduced from 0.8 to 0.5 nm. Below 0.5 nm, the AF coupling decreases due to the low spacer thickness, the occurrence of pinholes is expected, and consequently a direct FM coupling competes with the AF exchange coupling [FV02]. In these latter studies, however, no domain information was revealed.

3 Experimental techniques

This chapter focuses on the description of the sample preparation and on the main experimental techniques used to characterize the samples. In Section 3.1 the preparation of the samples is highlighted. In Section 3.2 and 3.3 Magnetic Force Microscopy (MFM) and Vibrating Sample Magnetometry (VSM), respectively, are described.

3.1 Sample preparation

The samples used in this work, Co/Pt/Ru and Co/Pt/Ir prepared on extended substrates and Co/Pd multilayers deposited on spherical particles were provided by Olav Hellwig (Hitachi GST) and Manfred Albrecht (Chemnitz University of Technology), respectively.

The Co/Pt/Ru and Co/Pt/Ir samples were deposited at ambient temperature on Si_3N_x coated Si substrates by magnetron sputtering using a con-focal sputter-up geometry in a ATC 2200 system from AJA International. A 20 nm Pt seed layer was used. During growth the samples were rotated at $\sim$ 5 Hz for better uniformity. The deposition rates were 0.1-0.2 nm/s. The sputtering was performed in 3 mbar Argon. Finally, the samples were covered with a 2 nm Pt layer to prevent oxidation. X-ray reflectivity and diffraction measurements confirm a well-defined multilayer structure with a (1 1 1) crystalline texture of the Pt buffer [Hel07].

Densely packed two-dimensional arrays of monodisperse spherical polystyrene particles in the size of 58 nm are formed by self-assembling upon slow evaporation of a solvent under ambient conditions. Such particle monolayers are typically used as a two-dimensional deposition mask for nanostructure fabrication followed by mask removal. The assemblies of polystyrene particles were covered with Co/Pd multilayer stacks with a different number of bilayers, N, ranging between 8 and 80. The deposition of $[\mathrm{Co}(0.27\ \mathrm{nm})/\mathrm{Pd}(0.8\ \mathrm{nm})]_N$ multilayer stacks was performed by magnetron sputtering using Kr as sputter gas at a pressure of 3.9×10^{-2} mbar. In order to improve the growth conditions of the multilayers, a 5 nm thick Pd buffer layer was sputtered onto a 1 nm thick Cr seed layer ($3.5\ \times10^{-2}$ mbar of Ar pressure) grown directly on the particles. A 1 nm thick Pd capping layer was additionally deposited to protect the sample from oxidation [Alb05a].

3.2 Magnetic force microscopy (MFM)

Magnetic force microscopy (MFM) is a special mode of operation of the scanning force microscope. The technique employs a magnetic tip, which is brought close to a sample surface (10-100 nm) and interacts with the magnetic stray fields near the surface. The strength of the local magnetostatic interaction determines the vertical motion of the tip as it scans across the sample. MFM was introduced shortly after the invention of atomic force microscopy [Mar87],

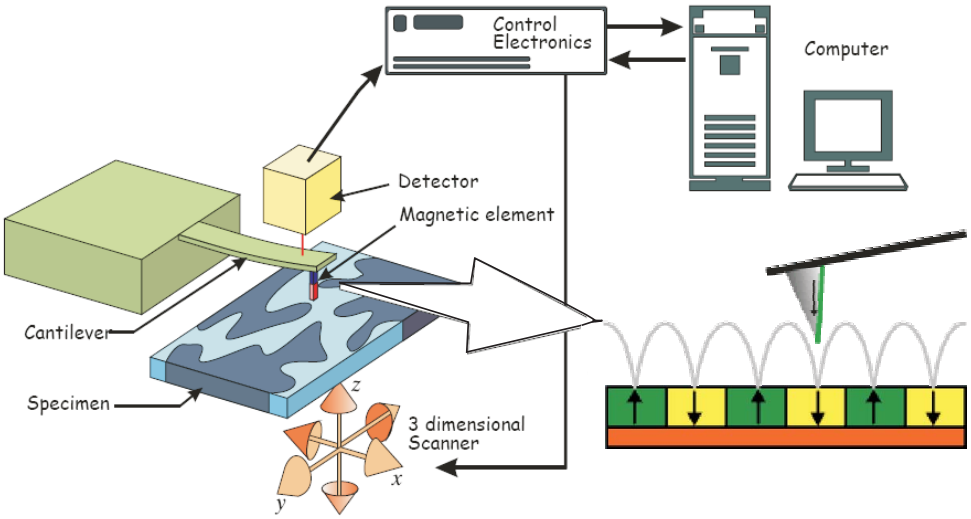

Fig. 3.1: Principle of Magnetic Force Microscopy [Hop05].

and became popular as a technique that offers high imaging resolution without the need for special sample preparation or environmental conditions. Since the early 1990s, it is widely used in the fundamental research of magnetic materials, as well as in the development of magnetic recording components.

The image is formed by scanning the tip laterally with respect to the sample and measuring the force (or force gradient) as a function of position. The concept is schematically illustrated in Fig. 3.1. That way, MFM can detect locally varying stray fields and gives therefore a qualitative picture of the sample domain structure.

Nowadays, the main developments in MFM are focused on the quantitative analysis of data, improvement of resolution, and the application of external magnetic fields during the measurements [Por98].

Basics of contrast formation

MFM is a non-contact technique, and both static and dynamic operating modes can be applied. The static mode detects the magnetic force acting on the tip, whereas the dynamic mode measures the force derivative acting on the tip. The force derivative is determined from a change in the dynamic properties of the cantilever, such as a shift in phase, oscillation amplitude or resonance frequency. Phase detection and frequency modulation give the best results, with a higher signal-to-noise ratio. These detection modes require the addition of an electronics module (Extender) to the Dimension Microscope. The signal depends on the force derivative in the following manner:

$$\Delta\Phi \sim -\frac{Q}{k}\frac{\partial F}{\partial z} \tag{3.1}$$

where Q is the quality factor and k is the cantilever spring constant.

An attractive interaction ($\frac{\partial F}{\partial z} > 0$) leads to a negative frequency shift, while a repulsive interaction ($\frac{\partial F}{\partial z} < 0$) gives a positive frequency shift. The force derivative can originate from a wide range of sources, including electrostatic tip-sample interactions, van der Waals forces, damping, or capillary forces. However, MFM relies on those forces that arise from a long-range magnetostatic coupling between tip and sample. This coupling depends on the internal magnetic structure of the tip, which greatly complicates the mechanism of contrast formation.

However, at short distances, it is difficult to separate the magnetic interactions from van der Waals interactions. Taking advantage of the fact that topographic interactions are short range while magnetic interactions are long range, one uses the "lift-mode" technique: take an image of the sample at short distances to obtain primarily topographic information, then use this information to keep the tip at a fixed height Δh above the sample, following the topography, and thereby obtain a (almost) purely magnetic image (Fig. 3.2).

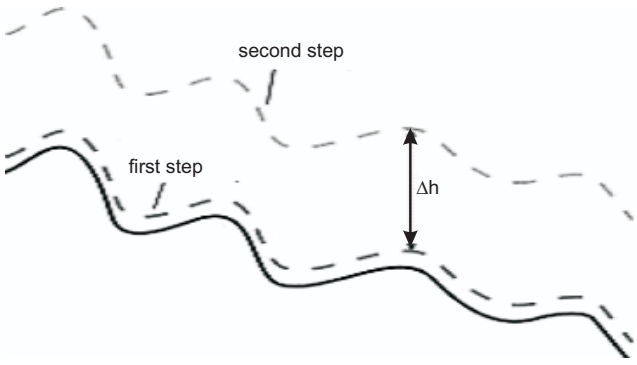

Fig. 3.2: Illustration of "lift-mode" principle.

MFM in field

In order to apply a perpendicular magnetic field to the sample during MFM measurements, a strong pyramidal stack of NdFeB permanent magnets with their texture axis perpendicular to the sample surface was lifted gradually to approach the sample from below. The full

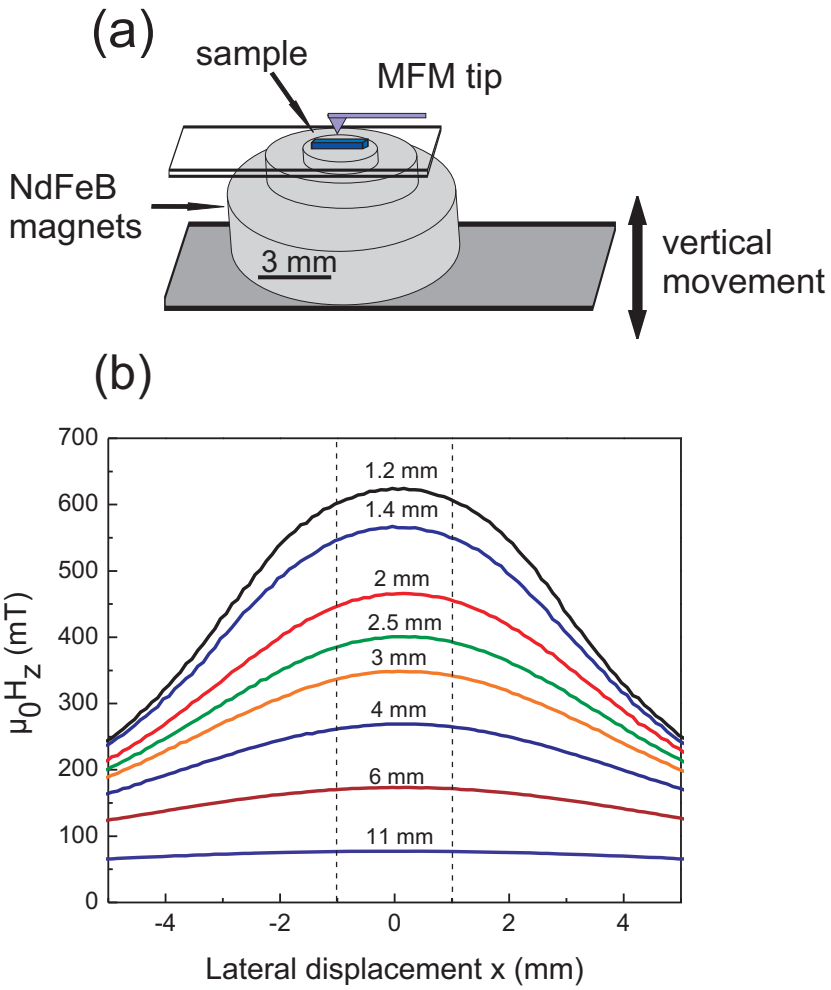

Fig. 3.3: (a) Schematic view of the MFM setup with NdFeB magnets, (b) Magnetic field H_z measured in lateral displacement, at different distances from the sample.

sample size (< 3 mm) is typically smaller than the smallest dimension of the magnet. The sample is placed with a precision of $\pm$ 0.5 mm above the center of the magnet, guaranteeing a perpendicular orientation of the field in the sample center (Fig. 3.3(a)). The field distribution above the permanent magnet was measured with a Mag-Scan Hall probe system. The lateral field homogeneity is better than 1 % within a radius of 1 mm from the center of the magnet, and the field strength in the central area can be varied from 0.02 T to a maximum of 0.6 T for a fully approached magnet (Fig. 3.3(b)).

3.3 Vibrating sample magnetometry (VSM)

Vibrating Sample Magnetometry (VSM) systems are used to measure the magnetic properties of materials as a function of magnetic field, temperature, and time. If a material is placed within an uniform magnetic field H, a magnetic moment m will be induced in the sample. In a VSM, a sample is placed within suitably placed sensing coils, and is made to undergo sinusoidal motion, i.e., mechanically vibrated. The resulting magnetic flux changes induce a voltage in the sensing coils that is proportional to the magnetic moment of the sample. The magnetic field may be generated by an electromagnet or a superconducting magnet. Variable temperatures may be achieved using either cryostat or furnace assemblies.
Field, temperature and time dependent magnetization measurements of Co/Pt-based multilayers were performed in a PPMS VSM setup (2 K $\leq$ T$\leq$ 400 K) with a maximum perpendicular field of 9 T. Additionally, VSM measurements were performed in an in-plane field up to a maximum field of 5 T. As an example, Fig. 3.4 shows the room temperature out-of-plane and in-plane hysteresis loops of Co/Pt/Ru multilayers.

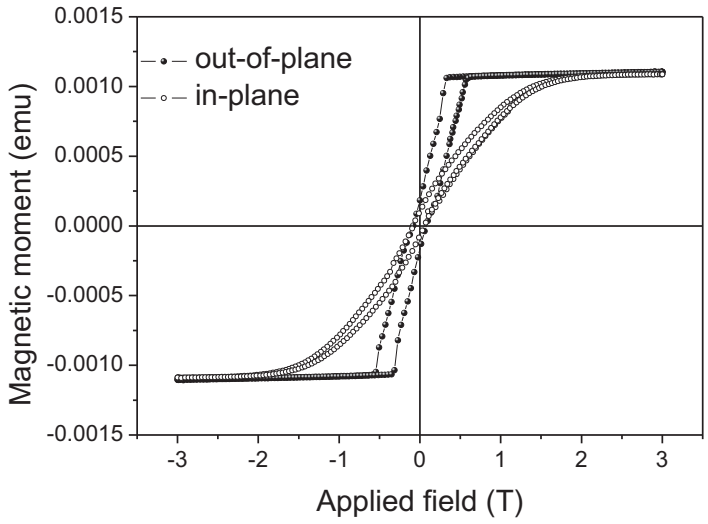

Fig. 3.4: Magnetic hysteresis of Co/Pt/Ru multilayers measured with PPMS VSM.

4 Band and bubble domains in [(Co/Pt)/Ru] multilayers

In recent years, the study of the antiferromagnetic (AF) interlayer coupling has been extended to ferromagnetic (FM) layers with perpendicular anisotropy [Hel03], which are of special interest for applications in perpendicular magnetic recording technology. One way of realizing such FM layers with perpendicular anisotropy is to utilize the interface anisotropy of a very thin Co film, either as a single layer or within a multilayer consisting of Co and Pt or Pd [Car85, Has89]. FM layers, separated by a thin non-magnetic spacer layer display an

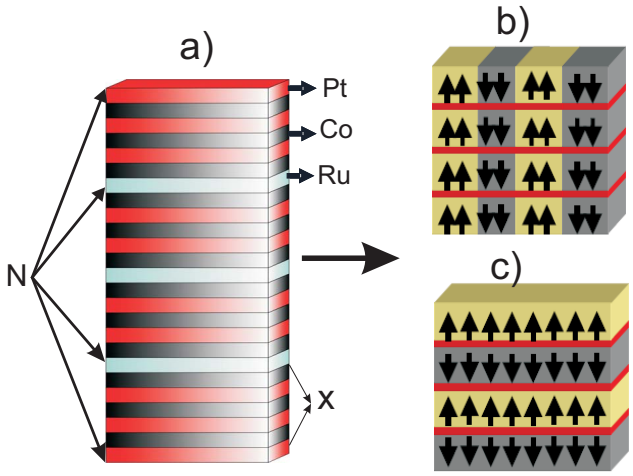

Fig. 4.1: Schematic view of (a) the sample architecture and two possible magnetic states (b) ferromagnetic, (c) antiferromagnetic.

oscillatory interlayer exchange coupling between FM layers. The interlayer exchange coupling is mediated by the Ruderman-Kittel-Kasuya-Yosida (RKKY) interaction, and determines the magnetic alignment of the FM layers (Section 2.2.2). In the well studied [Co/Pt]/Ru multilayer system [Hel07], which is composed of individual stacks of Co/Pt multilayers separated by thin Ru spacer layers (Fig. 4.1(a)), the balance of AF exchange coupling and dipolar coupling via the details of the multilayer architecture leads to a large variety of different magnetic zero field states, that are observed using domain imaging techniques. In the FM

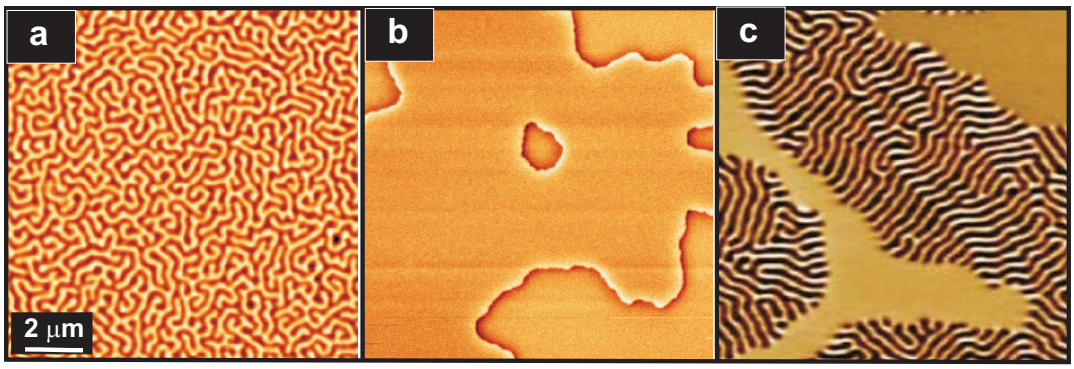

Fig. 4.2: MFM images of various types of domains as observed in AF-coupled Co/Pt/Ru multilayers. Image (c) taken from [Hel07]

band domain state (Fig. 4.1(b)), the perpendicular magnetization is correlated in vertical direction throughout the whole block, but forms neighboring domains with opposite magnetization direction in order to minimize the stray field energy very similar to the band domains discussed in Section 2.1.1. In the homogeneous AF state (Fig. 4.1(c)), the magnetization is laterally correlated in each individual Co/Pt block, but antiparallel from block to block in order to minimize the AF interlayer coupling. Examples for different possible states are summarize in Fig. 4.2. Picture (a) shows "up"-"down" band domains characteristic for the FM phase, (b) shows the AF dominated phase with a sharp antiphase boundary and (c) shows a mixed phase where the AF and FM domains coexist.

In this chapter, the domain structure and the magnetization processes are studied in a rather thick [Co/Pt]/Ru multilayer, which the zero field state is characterized by the above described FM band domains also common to simple single layer films with perpendicular anisotropy.

4.1 Experimental observation of strip-out and collapse field

In-field Magnetic Force Microscopy (MFM) measurements are performed to follow the evolution of the domain structure in a perpendicularly oriented magnetic field in the ascending and descending branch of the first quadrant of the magnetization curve. The qualitative similarity of the behavior to that of bubble domains known in single layer films [Thi70] [see Section 2.1.2] and multilayers without antiferromagnetic spacer layer [Rus01], suggests a possible description of the observed phenomena in these multilayers by a modified bubble theory. The multilayer system used for these experiments is $[(\mathrm{Co}(0.4\ \mathrm{nm})/\mathrm{Pt}(0.7\ \mathrm{nm}))_8/\mathrm{Co}(0.4\ \mathrm{nm})/\mathrm{Ru}(0.9\ \mathrm{nm})]_{18}$, which is in the following referred to as the [Co/Pt]/Ru multilayer.

Figure 4.3 shows the magnetization curve of the [Co/Pt]/Ru multilayer as a function of the

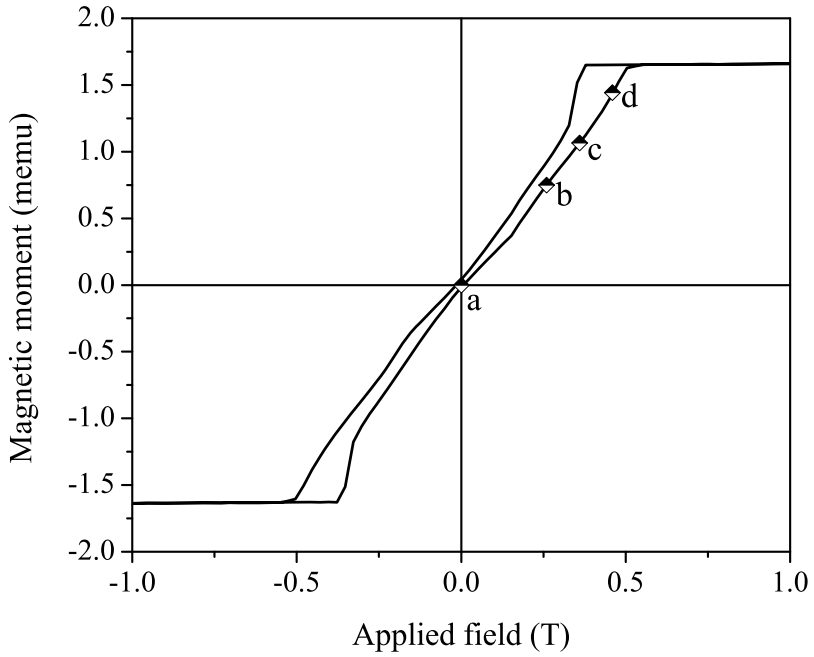

Fig. 4.3: Hysteresis loop of [Co/Pt/]/Ru multilayer measured by VSM with the field perpendicular to the sample surface. The points represent the field values used for the MFM measurements presented in Fig 4.5.

applied field, which is oriented perpendicular to the film plane. At zero applied field the film is in a nearly demagnetized state with a remanence close to zero. By increasing the field value, the magnetization increases almost linearly until it reaches saturation. At this point, the film is completely magnetized in the direction of the applied field. Reducing the field from positive saturation, the magnetization curve shows a kink in the first quadrant and, after that, abruptly reduces and continues to decrease with decreasing field. As the field is always parallel to the anisotropy axis, rotational processes are not expected in the magnetization reversal, thus the reversal is expected to happen via nucleation of reversed domains and their expansion until at large negative field the former positive domains are fully expelled from the film. From these out-of-plane measurements the values for the saturation polarization J_s= 0.765 T and the coercive field $\mu_0 H_c$= 0.01 T are extracted.

MFM images of the sample taken in three different remanent states are shown in Fig. 4.4. The dark and bright contrast corresponds to domains with magnetization pointing “up” and “down”, respectively. In the as-prepared state (Fig. 4.4(a)), the image is characterized by a labyrinth domain pattern. After out-of-plane saturation, the multilayers exhibit a random maze domain pattern as shown in the MFM image in Fig. 4.4(b). The average domain

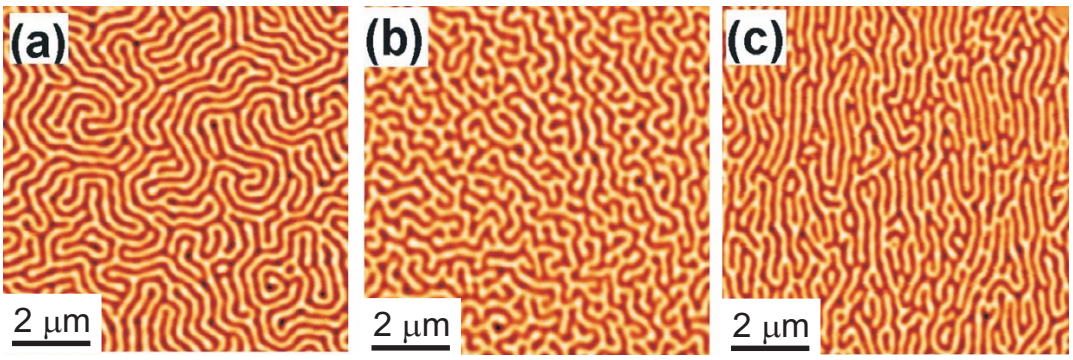

Fig. 4.4: MFM images of [Co/Pt]/Ru in three different remanent states: a) as-prepared state, b) after out-of-plane saturation, c) after in-plane ac-demagnetization.

width in both cases is about 180 nm. Applying a saturating in-plane magnetic field with subsequent in-plane AC demagnetization changes significantly the domain pattern, and the average domain width is reduced to about 135 nm. The in-plane magnetic field couples to the in-plane magnetization component of the domain wall and aligns the band domains parallel to the external field direction [Hub98] as it is visible in Fig 4.4(c). Numerical calculations of dipolar sums predict that the parallel stripes are energetically favored over a labyrinth domain or maze domain structure [PH92]. The above comparison, however, shows that the domain configuration in the remanent state depends strongly on the magnetic history, and the energetically lowest state has to be initiated by an appropriate demagnetizing procedure. Figure 4.5 shows a series of MFM images for different magnetic fields applied perpendicular to the sample plane during measurement. The as-prepared film was structured for an easier recognition of the scanned area. For the given structure with its geometry and size no influence of the lateral confinement on the domain configuration was observed. Thus, the presented results can be seen as representative for extended films. Starting from the demagnetized state, in fields which are small compared to the saturation field, the domains change very slowly. The first magnetizing process can be observed at the rim of the element where bright domains oriented parallel to the element edge disappear first. This can be understood from the unfavorably large magnetostatic energy for such oriented domains due to large stray fields [Neu04]. By increasing the external magnetic field, the domains which are aligned parallel to the field grow while the oppositely aligned domains get smaller. This process occurs gradually, until the domains transform into isolated stripes (Fig. 4.5(c)) and, in the end, into a bubble domain structure at higher fields (Fig. 4.5(d)). However, near the strip-out instability field (the field in which the elongated domains with opposite magnetization transform into bubble domains), a rapid growth of the preferably aligned domains can be

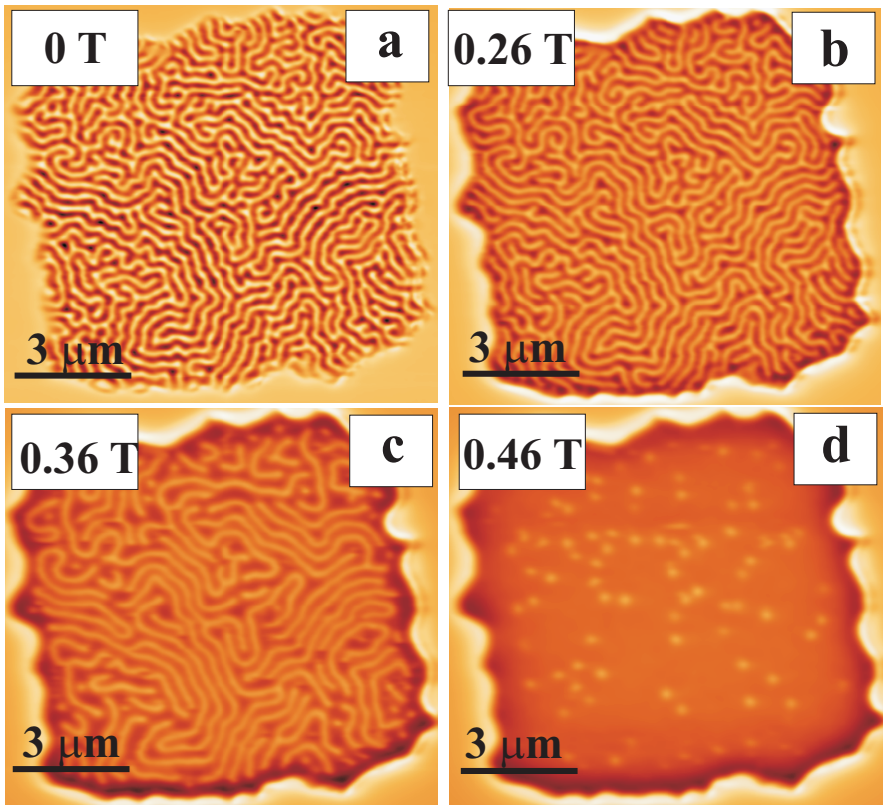

Fig. 4.5: Domain structures in a [Co/Pt]/Ru multilayer recorded along the increasing branch of the hysteresis.

observed. During this process, the width of the domains oriented opposite to the applied field remains nearly constant while they contract along their length [Eim00]. A further increase of the external field causes the bubbles to shrink until, at a critical field (collapse field) of 0.52 T, they collapse (not shown here). In order to obtain a more precise quantitative field value at which the strip-out instability occurs, a series of MFM images was recorded now on the decreasing branch of a minor loop in a narrow field range close to saturation (Fig. 4.6). This can ensure that the strip-out starts from isolated bubbles and is not influenced by the domain configuration at lower fields. Starting from the highest value where the bubbles still exist (0.5 T), upon decreasing the field, the bubble shape and configuration stay stable but the MFM contrast arising from the bubbles changes gradually down to 0.41 T.

This is best seen in exemplary MFM profiles extracted from the measurements across an individual, isolated bubble as a function of the applied field (Fig. 4.7). Both, the full width at half maximum and the absolute MFM contrast increase with decreasing field, which is interpreted as a continuous enlargement of the bubble. As described in the experimental section, MFM records only the force gradient experienced by a magnetic tip due to the magnetostatic interaction with the z-component of the bubble stray field. The contrast,

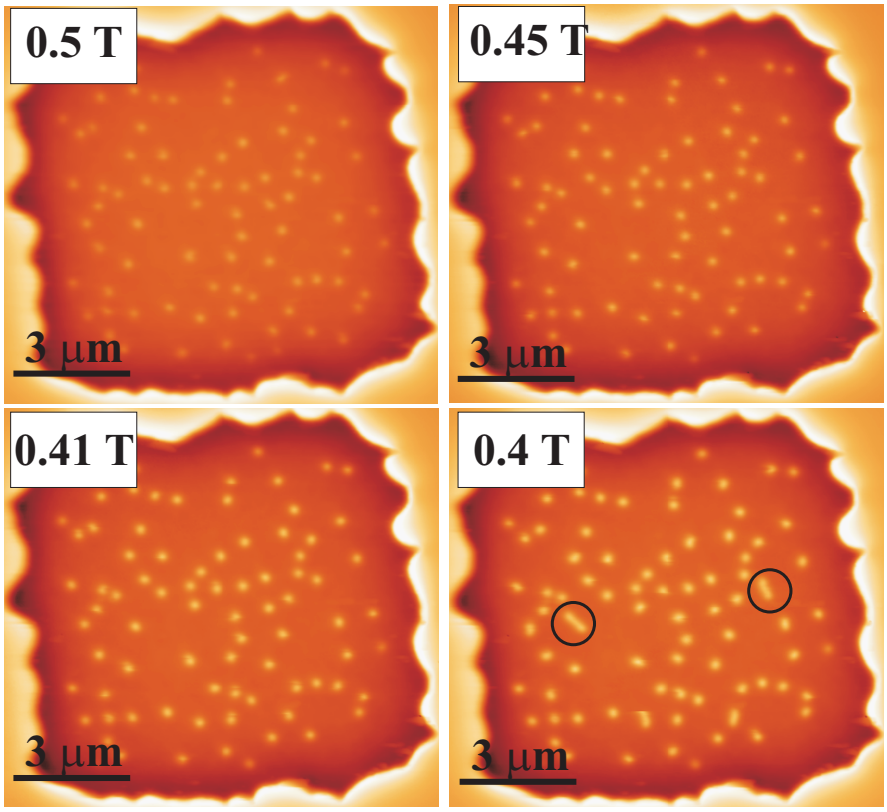

Fig. 4.6: Sequence of MFM images of [(Co/Pt)/Ru] multilayers recorded on the decreasing branch of a minor loop.

therefore, also largely depends on the magnetic structure and the volume of the tip coating and is necessarily broadened compared to the true size of the bubble. Thus, one cannot conclude on the exact bubble diameter from MFM measurements with an uncalibrated tip. At 0.4 T (strip-out field) the instability occurs and the bubbles start to expand into isolated stripes (Fig. 4.6 (circled with dark blue)).

4.2 Comparison between the theoretical model and experimental results

The observed magnetization processes resemble those seen in single layer thick films with perpendicular anisotropy (Section 2.1.2). Close to saturation, the labyrinth band domains contract to form isolated stripe domains and transform further into bubble domains. In this state, bubble domains can either transform back into isolated stripes by reducing the field below H_{bs} (the bubble strip-out field) or can collapse when increasing the field above H_{bc}. A. N. Bogdanov and co-workers in the IFW Dresden, have extended the bubble theory described

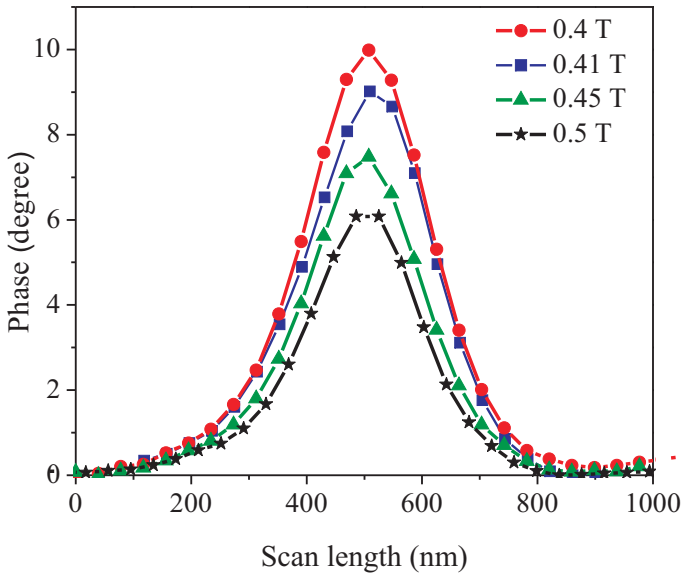

Fig. 4.7: MFM profile of an isolated bubble for different applied fields.

in Section 2.1.2 to calculate the critical bubble diameters and fields also for coupled multilayers as observed in the experiment. The only adapted parameter is the characteristic length l_c= 4.43 nm. This value has been derived from analysis of the domain periods measured in series of $[\mathrm{Co}(0.4\ \mathrm{nm})/\mathrm{Pt}(0.7\ \mathrm{nm})]_X$ multilayers [Dav04].

A multilayer system consisting of $N^* = NX$ identical magnetic layers with magnetization

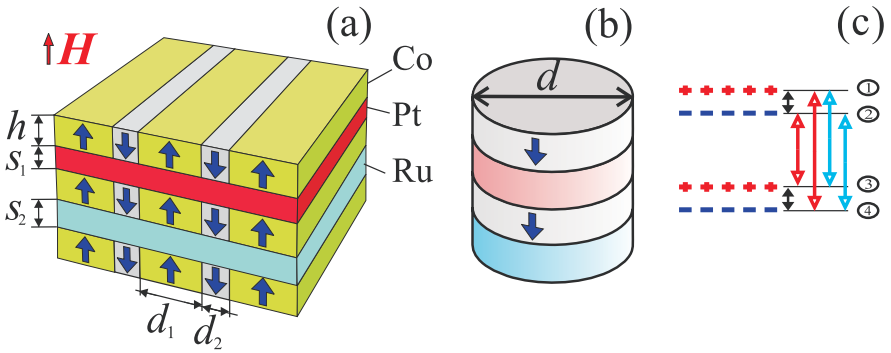

Fig. 4.8: (a) A fragment of multilayers with band domains, (b) an isolated bubble, and (c) contribution of the magnetostatic interaction between two layers.

M and thickness h separated by spacer layers of thickness s_i is considered (Fig. 4.8(a)). For every X magnetic layer, the separating spacer layer mediates an AF coupling. Generalizing the results of Kiselev et al. [Kis07, Kis08] the energy of the band domain phase for one layer

is:

$$E = \frac{2J_s}{\mu_0}\frac{l_c}{D} + \frac{J}{h}\left(1 - \frac{1}{N}\right) - HJ_s q + \frac{J_s^2}{2\mu_0}\tilde{N}(D,q) \tag{4.1}$$

where $D = d_1 + d_2$ is the band period, $q = (d_1 - d_2)/D$ is the domain imbalance, $J > 1$ the antiferromagnetic exchange interaction coupling constant, and $l_c = \mu_0\sigma/J_s^2$ the characteristic length, defined by the ratio of wall energy density σ and magnetostatic energy density $J_s^2/2\mu_0$. The first term in Eq.(4.1) describes the wall energy density of the FM band domain pattern, the second term quantifies the antiferromagnetic exchange energy, which has to be paid at all $N - 1$ Ru containing interfaces. The third term (Zeeman term) lowers the energy when domains grow with the magnetization parallel to the field. The remaining stray field energy density is expressed with the help of an effective demagnetizing factor:

$$\tilde{N}(D,q) = \tilde{N}_{self}(D,q) + \tilde{N}_{interaction}(D,q) \tag{4.2}$$

which includes the self energy of individual magnetic layers and the interaction between them (Fig. 4.8(c)) [Bra09]. The equilibrium parameters of the stripes are derived by a minimization of the energy according to Eq (4.1) with respect to D and q and result in $D_0 = 264.3$ nm for the band domain period, which is very close to the observed band period of 270 nm after in-plane AC demagnetization (see Fig. 4.4). Considering now an isolated bubble of

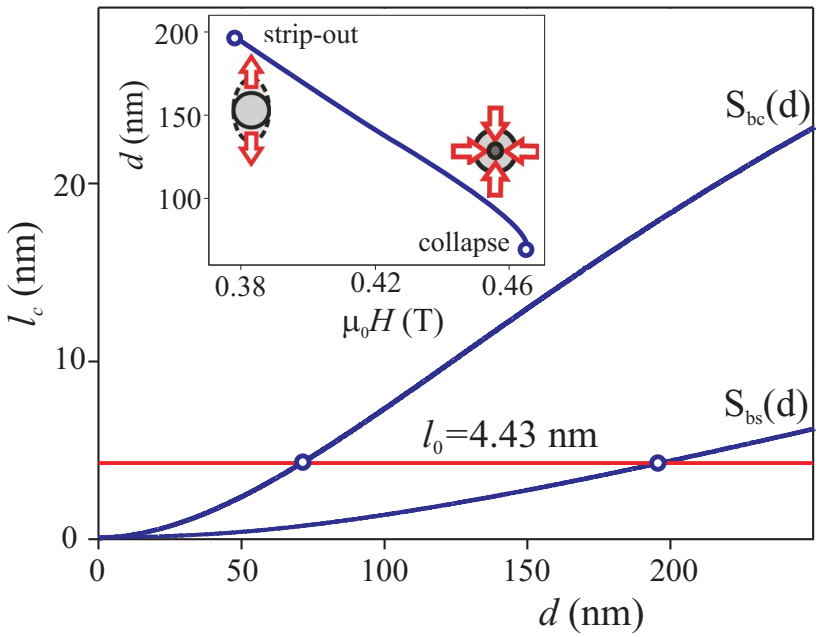

Fig. 4.9: The characteristic functions $S_{\mathrm{bc}}(d)$ and $S_{\mathrm{bs}}(d)$ determine bubble sizes at collapse (d_{bc}) and strip-out (d_{bs}) fields. For [Co/Pt]/Ru multilayers ($l_c = 4.43$ nm) $d_{\mathrm{bc}} = 69.76$ nm and d_{bs}= 193.47 nm were obtained. The inset shows the equilibrium values of the bubble diameters as a function of the bias field.

diameter d (Fig. 4.8(b)), the total energy can be written as a sum of the wall energy, the Zeeman energy and the magnetostatic energy [Bra09]. Following the standard methods (see e.g. Ref.[Hub]) one can derive the critical parameters of the bubble existence based on the two stability criteria (outlined in Section 2.1.2). The equation $S_{\mathrm{bc}} = l_c$ defines the critical minimum diameter (collapse diameter) d_{bc}, down to which an isolated bubble is stable for a film with given architecture and materials properties (l_c). Furthermore, the analysis of elliptical distortion results in an upper critical diameter d_{bc}, defined by $S_{\mathrm{bs}} = l_c$, above which a cylindrical bubble will elongate and transform into a stripe (strip-out diameter).

Within the limits given by d_{bc} and d_{bs} a cylindrical bubble is stable and its size is an unambiguous function of the external field according to equation:

$$l_c h + \frac{\mu_0 H h d}{J_s} - F(d) = 0 \tag{4.3}$$

where F(d) is called *force function* and represents the derivative of the stray field energy of bubbles [Hub98]. For the studied multilayer with $X = 9$ and $N = 18$ the stability functions are given in Fig. 4.9 in dependence of the diameter d and their intersection with l_c results in strip-out and collapse diameter. The insert shows the variation of d within the stability region as a function of the applied field. For the present [Co/Pt]/Ru multilayers it was estimate: $\mu_0 H_{\mathrm{bs}} = 0.38$ T and $\mu_0 H_{\mathrm{bc}} = 0.47$ T, values which are in good agreement with the experimental ones: $\mu_0 H_{\mathrm{bs,exp}} = 0.4$ T and $\mu_0 H_{\mathrm{bc,exp}} = 0.52$ T.

In summary, the magnetization process of AF-coupled [Co/Pt]/Ru multilayers with perpendicular anisotropy was studied by direct MFM observation. The magnetization proceeds as typical for single layer thin films with perpendicular anisotropy via gradual growing of domains oriented in the same direction with the applied field and contracting of those oriented opposite to the applied field. Strip-out and collapse fields have been determined from domain imaging in narrow subsequent field steps. In collaboration with the theory group in IFW a micromagnetic theory was developed that treats band and bubble domains in multilayer films with small individual layer thicknesses that consequently was applied to the experimentally studied multilayer architecture. The comparison between experimental results and the theoretical model showed very good agreement.

5 Metamagnetic domains in AF-coupled [(Co/Pt)/Ru] multilayers

In Chapter 4 the magnetization process of $[(Co/Pt)_{X-1}/Co/Ru]_N$ multilayers with X=9 and N=18 was investigated via MFM at room temperature by imaging the domain configuration in magnetic fields. At room temperature the samples show band domains which are characteristic of the ferromagnetic state.
The present chapter focuses on $[(Co/Pt)_{X-1}/Co/Ru]_N$ multilayers with X=8 and N=18, where at room temperature the AF exchange coupling dominates, leading to an antiparallel alignment between adjacent FM stacks. In order to investigate field and temperature dependent magnetization reversal, in-field domain imaging and magnetic measurements have been performed.

5.1 In-field domain observation

The reversal modes in $[(\mathrm{Co/Pt})_{X-1}/\mathrm{Co/Ru}]_N$ multilayers with X=8 and N=18 are determined by the relative strength of the AF coupling compared to the remaining energy terms. This can be tuned by sample thickness, temperature or magnetic field.

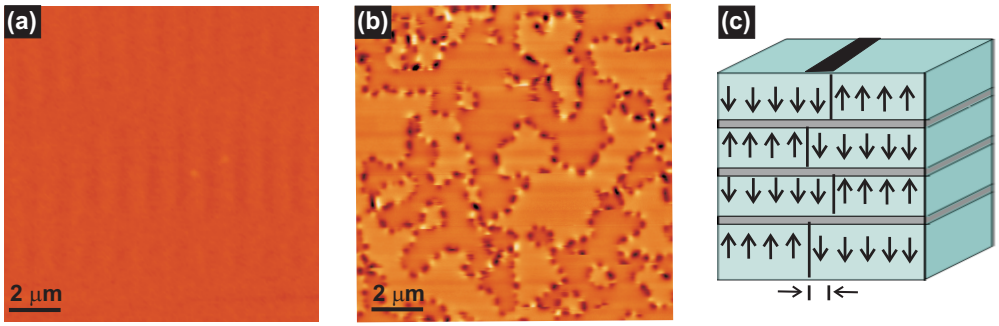

Fig. 5.1: MFM images of the remanent state after (a) out-of-plane saturation and (b) in-plane saturation . (c) Illustration of shifted reversal as observed in (b), here for N=4.

Figure 5.1 shows the MFM images after out-of-plane saturation (a) and after in-plane

saturation (b), respectively. Out-of-plane saturation puts the system into the homogeneous AF-coupled state, with no magnetic domains, while in-plane saturation creates large AF-domains separated from each other by anti phase boundaries, which in the present case are of a special ferromagnetic type with "up"-"down" modulation (so called "tiger-tails"). The large AF domains result from the full saturation in plane, upon which the AF coupling between neighboring stacks and the alignment parallel to the anisotropy axis is destroyed. Decreasing the applied field back to zero leads to a tilting of the magnetization in each stack back into the perpendicular direction simultaneously obeying the AF alignment. This, however, can occur locally with a different polarity sequence and leads to antiphase boundaries as in Fig. 5.1 (b). Additionally, due to the large interlayer exchange, the AF domain walls are not perfectly aligned vertically from stack to stack but possess an alternating right/left shift. The shift produces a FM band at the AF boundaries in which the magnetization of each stack is aligned vertically, as shown schematically in Fig. 5.1 (c). At this point the dipolar fields increase and in order to minimize this energy the FM band breaks up into "up"-"down" domains along its length [Kis07].

Figure 5.2 shows a systematic temperature study for $[(Co/Pt)_7/Co/Ru]_{18}$ multilayers with

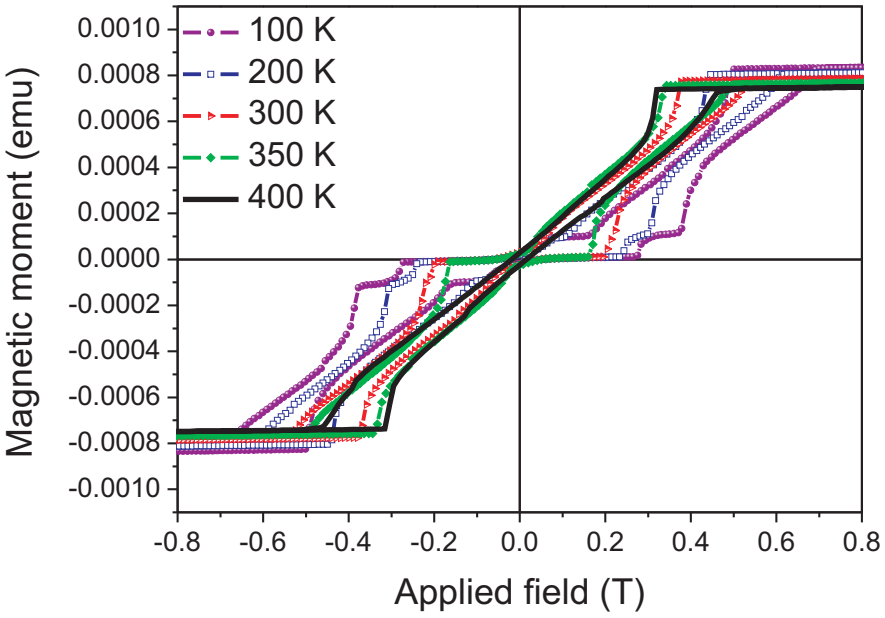

Fig. 5.2: Hysteresis loops for $[(Co/Pt)_{X-1}/Co/Ru]_N$ multilayers with X=8 and N=18 at different temperatures.

out-of-plane measurements for 100, 200, 300, 350 and 400 K. For low temperatures a characteristic feature is a plateau in the magnetization around zero field which is due to the AF ground state. The step-like increase is interpreted as the breaking up of the AF coupling in the external field. At 100 K the AF coupling is strongest and a double stepped hysteresis loop is observed with the first reversal at about 0.27 T and the second at 0.37 T. At 200 K, the AF coupling is reduced and the reversal occurs at about 0.23 and 0.3 T, respectively. At 300 K, the hysteresis loop displays only one step at 0.2 T and, by increasing the temperature to 350 K, the step is shifted to 0.15 T. Finally, at the highest temperature (400 K) the step vanishes and the shape of the curve suggests a ferromagnetic behavior. The multiple steps in the hysteresis for T<300 K suggest a stack-by-stack reversal with an AF state at remanence. As function of temperature, the sample exhibits both vertically and laterally correlated magnetization reversal modes. At high temperatures (400 K), a reversal via FM band domains is observed. At low temperatures the AF coupling dominates and gets stronger for lower temperatures.

To study in detail the reversal mechanism, measurements were performed at 300 K accessi-

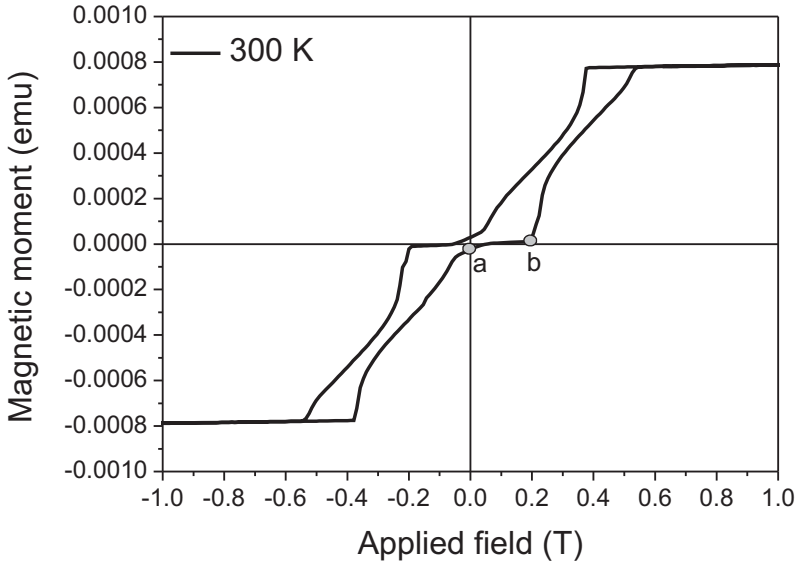

Fig. 5.3: Hysteresis loop measured by VSM with the field perpendicular to the sample surface.

ble with the microscope. Figure 5.3 shows the hysteresis loop of the sample measured at 300 K with the magnetic field applied perpendicular to the sample surface. At small magnetic fields, the sample displays a plateau (a-b) in which the magnetization of Co/Pt stacks align in an antiferromagnetic configuration (schematically presented in Fig. 4.1 (c)) along the easy

axis and is therefore less susceptible to the applied field. Increasing the field value above 0.2 T the antiferromagnetic coupling strength is overcome which leads to a step-like increase in magnetization.

For higher fields, the magnetization increases almost linearly until it reaches saturation. In

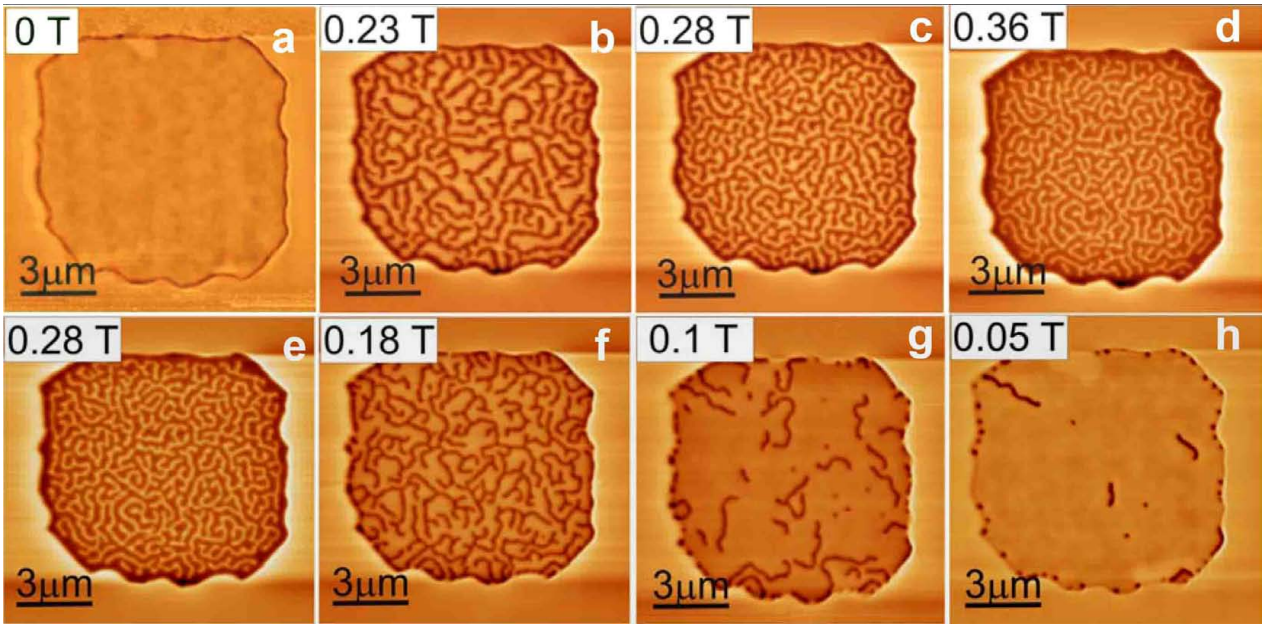

Fig. 5.4: Domain structures of $[(Co/Pt)_7/Co/Ru]_{18}$ multilayers measured by MFM as a function of a perpendicular magnetic field.

the field region of 0.2 T to 0.6 T a mixed state is expected, which is studied in more detail by in-field MFM observation.

The MFM images in Fig. 5.4 show the domain evolution with magnetic field starting from the AF state (Fig. 5.4(a)). Applying small fields, the initial AF state is preserved which corresponds to region a-b in Fig. 5.3. Starting with 0.2 T, the plateau is overcome and band-like FM "up" domains which form in the otherwise antiferromagnetic matrix (this state will be later called *metamagnetic domain*), and are aligned in the same direction as the applied field (Fig. 5.4(b)). Increasing the magnetic field further, the FM domains expand and the AF state becomes less predominant until finally being annihilated (not shown here). By decreasing the field (Fig. 5.4 (e-h)), the FM band state becomes unstable and the AF state becomes more and more predominant at small fields.

The magnetic hysteresis loop at 400 K (Fig. 5.2 (solid line)) indicates that at this temperature the reversal is mediated by band domains that couple through the entire thickness of the sample such as observed in Chapter 4. Consequently, the remanent state at 400 K is expected to be in the FM band domain state.

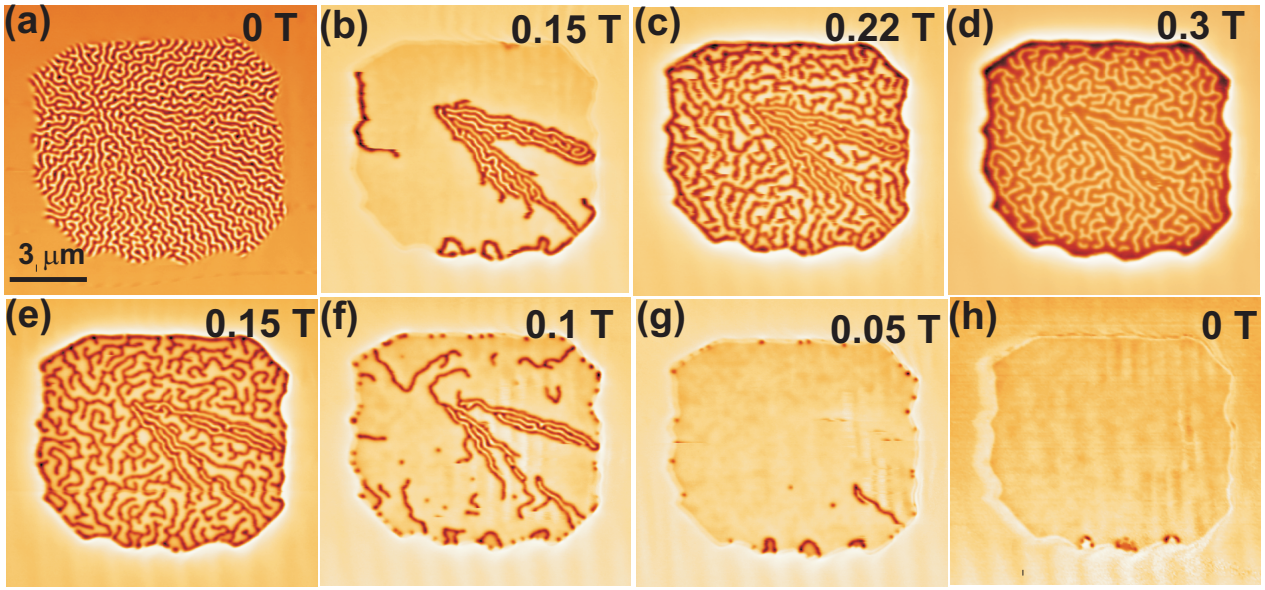

Fig. 5.5: Sequence of MFM images in perpendicular field, showing a two phase behavior of $[(Co/Pt)_7/Co/Ru]_{18}$ multilayers.

Figure 5.5 shows eight MFM images recorded at room temperature after the sample was previously magnetized in a positive field at 400 K. In the zero field state (Fig. 5.5(a)), the demagnetized sample shows FM band domains. It is deduced that the equilibrium domain state from 400 K is maintained upon cooling to room temperature, now, however, as a metastable state. As the magnetic field increases (Fig. 5.5(b)), a sudden transition from the metastable FM state into the stable AF state occurs. Similar to the case presented in Fig. 5.4, above 0.2 T additional "up" FM domains nucleate and propagate into the AF region. Increasing the field further results in a pronounced widening of the FM domains (Fig. 5.5(d)). By decreasing the field the AF state starts to grow until it finally covers the whole scanned area (Fig. 5.5(h)). At this point the sample is in its equilibrium state.

5.2 Magnetic phase diagram for metamagnetic domains

The theoretical model developed by A. N. Bogdanov and co-workers (IFW Dresden) (Chapter 4) was applied to $[(Co/Pt)_{X-1}/Co/Ru]_N$ multilayers with X=8, N=18. In a magnetic field, the AF phase transforms into the saturated state via a specific multidomain phase. This is similar to a metamagnetic phase transition in bulk antiferromagnets [Str77]. In an intermediate metamagnetic phase ferromagnetic "up" domains (see Section 5.1) form in the AF matrix. In the following these domain states are referred to as *metamagnetic domains*. For a multilayer formed by identical FM stacks the AF coupling of internal stacks is twice as

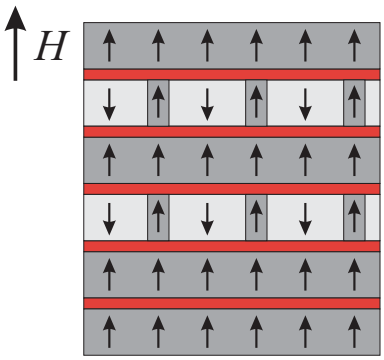

Fig. 5.6: Schematic view of multilayers (N=6) with metamagnetic domains.

large as for the top or bottom stack. Therefore, the reversal in a field might happen in 2 steps, that the surface stack can switch first and the internal stacks afterwards. This process starts gradually by reversing the domains oriented antiparallel to the applied field (Fig. 5.6). Due to the long-range magnetostatic coupling the domain walls are vertically correlated through all stacks. To find the equilibrium domain state, the total energy density has to include the domain wall energy, the interlayer exchange energy E_{ex}, the stray field energy E_d, and the Zeeman energy. It can be shown that the AF interlayer exchange coupling connecting ferromagnetic stacks acts as a bias field. Consequently, an *exchange bias field* is introduced into the Zeeman term:

$$H_{ex} = \frac{4\pi\alpha J}{hXJ_s} \tag{5.1}$$

where J is the strength of the AF interlayer exchange coupling and α is a factor corresponding to the surface and internal metamagnetic domains, respectively.
Similar to Chapter 4, the equilibrium domain sizes are derived by the minimization of the total energy with respect to the domain period, D and the imbalance of "up" and "down" domains, q.

The phase diagram in Fig. 5.7 shows six possible magnetic phases labeled as (I)-(VI) in the multilayer with N = 18 and different values of X. The phase diagram displays how the multidomain states change for the experimentally studied multilayers with X = 8 (Section 5.1), and 9 (Section 4.1). For a large thickness of the ferromagnetic block, the multilayer remains in the ferrostripe regime (VI) for all applied fields until the sample saturates (V). For the studied geometry this behavior is expected for X = 9 and larger. Multilayers with a smaller number of layers (X=5, 6) show a two-step magnetization behavior with a pronounced plateau at M = 0 for small fields until the surface layer switches through a surface metamagnetic transition in a small field range (II). This is followed by a second plateau (III) that marks the existence range of the surface metamagnetic domains. Then the well separated bulk

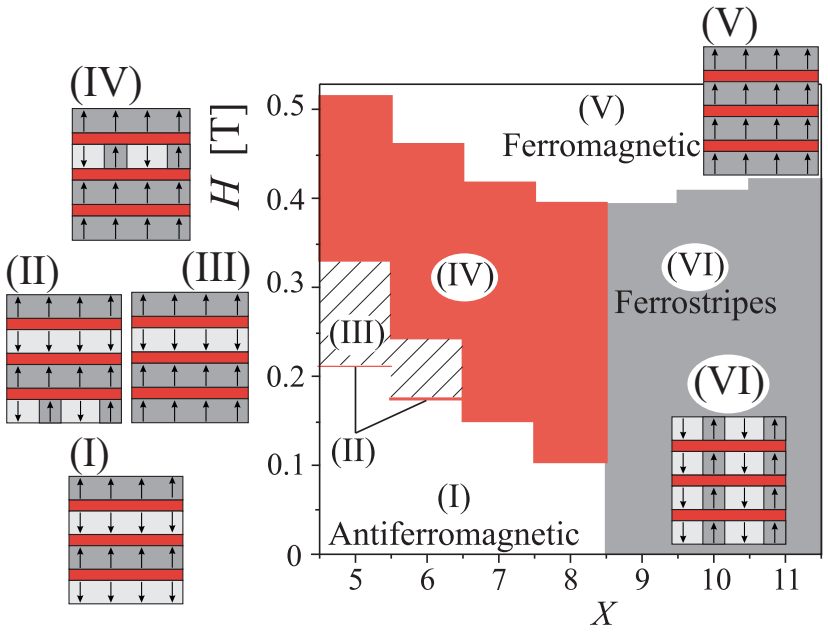

Fig. 5.7: Phase diagram.

metamagnetic transition follows. Here, stripe domains exist alternatingly in internal layers of the multilayer stack, as sketched in Fig. 5.6. For an intermediate thickness (X = 7, 8) surface and bulk metamagnetic transitions merge. Thus, only a single-step magnetization process is observed when the field overcomes the AF coupling. In those cases, the surface and the internal metamagnetic domain structures show a mixed appearance in accordance with the MFM observations in Fig. 5.4. These theoretical results match very well with exemplary hysteresis curves presented in Fig. 5.8. Calculated magnetization curves for X=7, 8 and 9

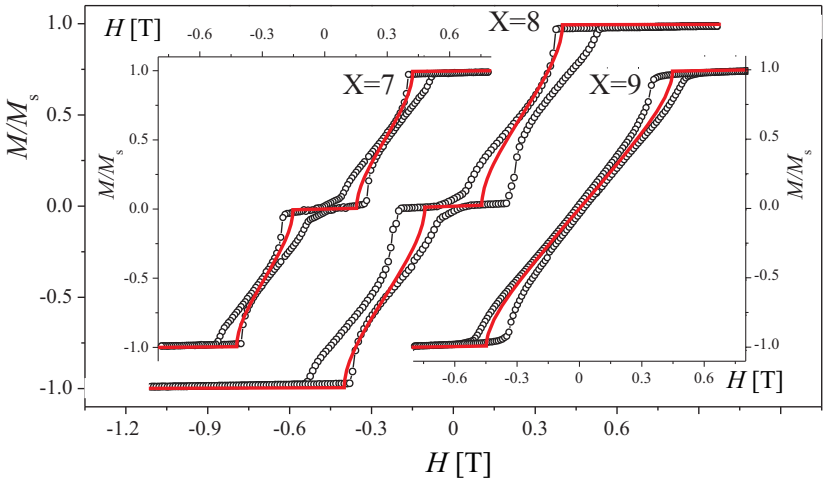

Fig. 5.8: Magnetization curves of $[(\mathrm{Co/Pt})_{X-1}/\mathrm{Co/Ru}]_{18}$ for X=7, 8 and 9, measured by VSM with the field perpendicular to the film plane (open symbols). Solid lines correspond to the theoretically calculated magnetization curves.

are plotted in Fig. 5.8 together with the experimental curves measured at 300 K with the field perpendicular to the film plane. The calculated curves are in good agreement with the experimental ones, showing for X=7 and 8 a plateau at M=0, and a purely FM behavior for X=9.

In summary, the magnetization processes of perpendicular AF-coupled $[(\mathrm{Co/Pt})_{X-1}/\mathrm{Co}/\mathrm{Ru}]_{18}$ multilayers, with X=8 were investigated by MFM. In such samples it was possible to alter the magnetic correlations from horizontal (AF state) to vertical (FM state) and vice versa via magnetic field cycling or temperature variation. Applying a field in the perpendicular direction, the AF state transforms into the saturated state via formation and expansion of metamagnetic domains.

The magnetization reversal of AF-coupled multilayers has been investigated as a function of temperature in the range of 100 - 400 K. The AF-coupling gradually decreases with increasing temperature, before it abruptly vanishes at 400 K.

Metamagnetic domains can be described by a modified model of FM domains (manuscript submitted to Phys.Rev. B). This allows to derive the equilibrium parameters of metamagnetic domains and calculate the magnetic phase diagram. The calculated phase diagram predicts the existence of three possible types of metamagnetic domains depending on the thickness of the ferromagnetic stacks, X, which is in good agreement with the experimental results.

6 Magnetization processes in AF-coupled [(Co/Pt)/Ir] multilayers

The magnetization reversal process in Co/Pt-based systems usually involves the formation of vertically correlated band domains through the entire multilayer film stack resulting from a competition between ferromagnetic (FM) exchange, anisotropy and dipolar energies. The energy balance was furthermore tailored by the addition of Ru spacer layers with appropriate thicknesses, which establishes antiferromagnetic (AF) interlayer exchange coupling (Chapter 4 and 5). The various reversal modes are determined largely by the sample geometry, the magnetization and the strength of the AF interlayer coupling. To study the

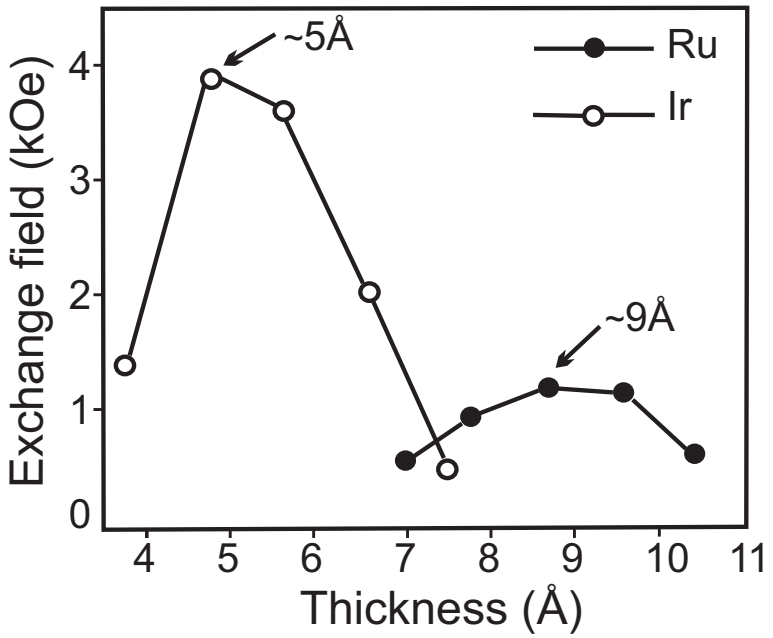

Fig. 6.1: Exchange coupling versus multilayer thickness for Ru and Ir spacer layer [Hel07].

magnetization process in systems with larger AF-coupling, Ru layers were substituted by Ir spacer layers, which is known to exhibit a larger induced AF-coupling ($\approx$ 3 times larger than Ru) [Hel07]. The detailed dependence of AF exchange field on the thickness of Ir and Ru spacer layers is given in Fig. 6.1 for a sample with N=2 and X=5 [Hel07]. The maximum AF

exchange field is obtained for 0.9 nm Ru and 0.5 nm Ir spacer layer thicknesses.

This chapter presents the magnetization results of $[(\mathrm{Co}(0.4\ \mathrm{nm})/\mathrm{Pt}(0.7\ \mathrm{nm}))_{X-1}/\mathrm{Co}(0.4\ \mathrm{nm})/\mathrm{Ir}(0.5\ \mathrm{nm})]_4$ multilayers made up of four $(\mathrm{Co/Pt})_{X-1}/\mathrm{Co}$ stacks with perpendicular anisotropy. Each stack is AF coupled through an Ir layer to the adjacent stack. Similar as in the Ru systems (see Chapter 4) for a small value of X, the films display an AF ground state with the moments of adjacent Co/Pt stacks aligned antiparallel to each other. Increasing X results in a transition to the FM stripe domain state [Hel07].

Magnetization processes in $[(\mathrm{Co/Pt})_{X-1}/\mathrm{Co/Ir}]_4$ multilayers with X=20

An out-of-plane magnetization curve for $[(\mathrm{Co/Pt})_{19}/\mathrm{Co/Ir}]_4$ multilayers is shown in Fig 6.2. In the zero field state the sample is almost demagnetized. With increasing field, the magnetization curve shows a continuous behavior up to saturation. The measurement reveals that

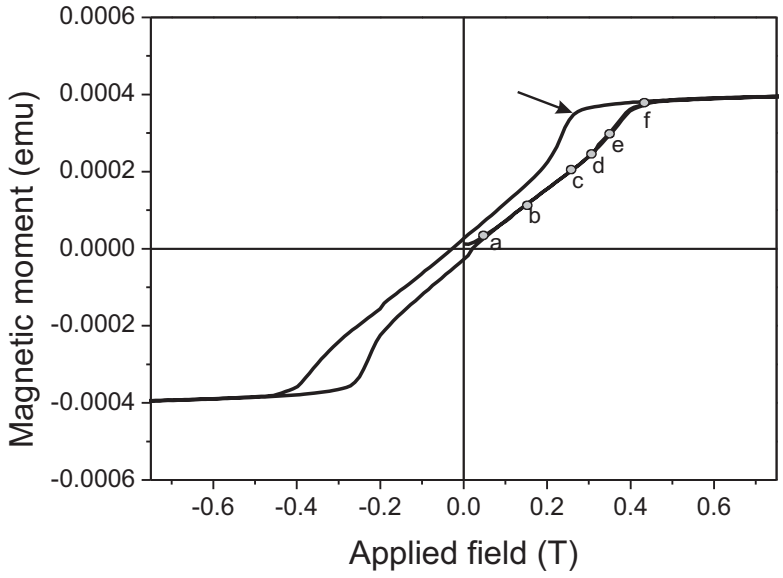

Fig. 6.2: Hysteresis loop measured by VSM with the field perpendicular to the sample surface. The points correspond to the field values applied in MFM measurements (Fig. 6.3).

the saturation field of the sample is ≈ 0.45 T. By decreasing the field, the magnetization curve shows a kink, marked by an arrow (≈ 0.25 T), and after that continues to decrease with decreasing field. The shape of the magnetization curve is typical of magnetic thin films with perpendicular anisotropy and seems to be characterized by nucleation and domain wall motion [Koo60]. The sample shows a similar behavior as the $[(\mathrm{Co/Pt})_8/\mathrm{Co/Ru}]_{18}$ multilay-

ers presented in Chapter 4. Figure 6.3 shows a series of MFM images, over a 15 μm^2 ×

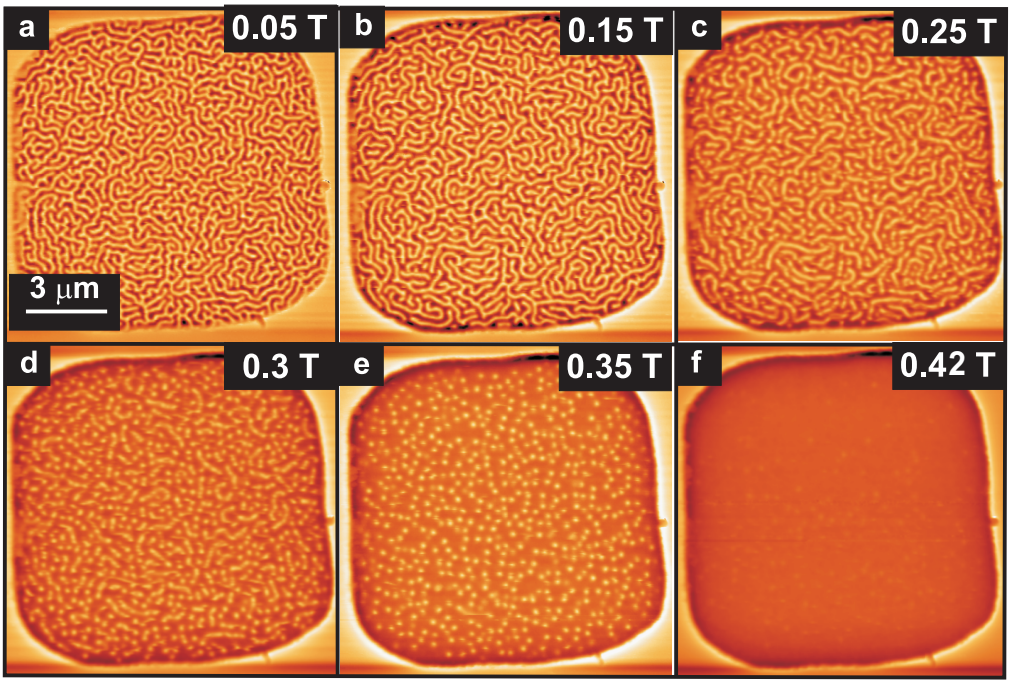

Fig. 6.3: Domain structures of $[(Co/Pt)_{X-1}/Co/Ir]_N$ multilayers with X=20 and N=4 measured by MFM in perpendicular magnetic field on the increasing branch of the hysteresis.

15 μm^2 area, taken along the increasing branch of the hysteresis loop. Initially, the sample was fully saturated in a positive 3 T out-of-plane field. In the zero field state, the sample shows a random maze domain pattern (Fig. 6.3(a)). The dark-bright contrast corresponds to "up"-"down" domains. The average domain width is about 130 nm. As the magnetic field is applied, the domains aligned parallel to the field grow, while the domains aligned opposite to the field contract along their lengths. At 0.25 T isolated stripe domains and bubble domains coexist (Fig. 6.3(c)). Increasing the field further the remained isolated stripes contract into bubbles. Approaching saturation (Fig. 6.3(e)), the bubbles reduce their diameter with increasing field, until at a critical field of $\mu_0 H_{bc}$=0.42 T (collapse field), they collapse (see Chapter 4).

After the sample was saturated, a MFM series was recorded along the decreasing branch of the hysteresis (Fig. 6.4). The field is decreased to 0.25 T where isolated nucleation of a few reverse domains (Fig. 6.4(b)) was observed, occurring at the marked kink in the hysteresis loop (Fig. 6.2). The nucleated domains grow in size with decreasing field. As the field is further reduced the small domains expand into isolated stripes. At 0.2 T (Fig. 6.4(c)) an expansion of maze domains is observed, seeded from the few nucleated domains already present. These domains expand through the whole scanned area very fast (Fig. 6.4 (d)-(e)).

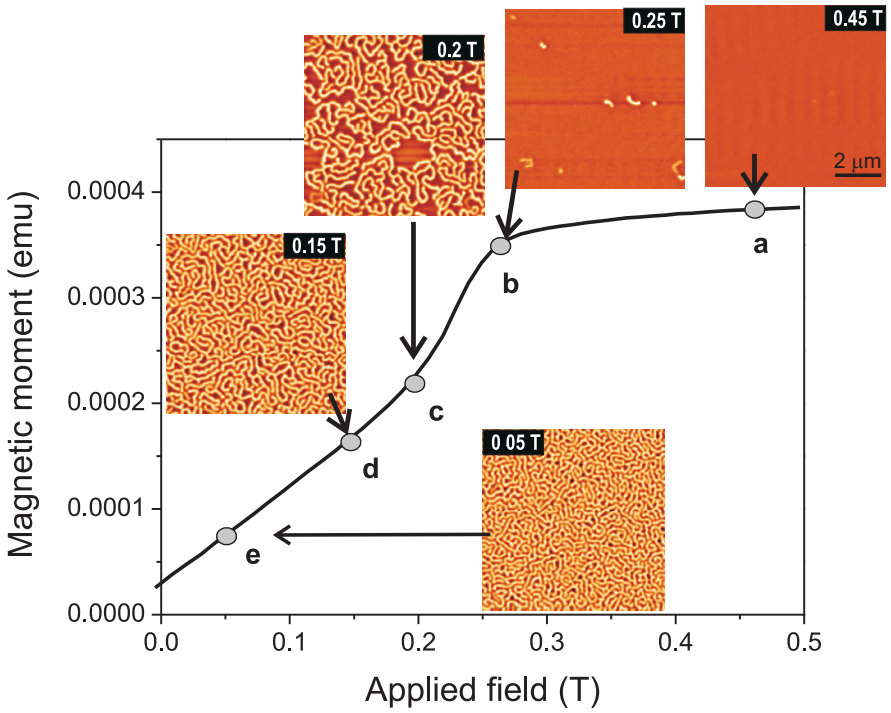

Fig. 6.4: Domain structures of $[(\mathrm{Co/Pt})_{X-1}/\mathrm{Co/Ir}]_N$ multilayers with X=20 and N=4 measured by MFM on the decreasing branch of the hysteresis.

In order to determine the strip-out field at which the bubbles transform into isolated stripes, a new series of MFM images was recorded now on the decreasing branch of a minor loop in a field range close to saturation. Starting from the bubble state (Fig. 6.3(e)) the field is reduced to 0.3 T when the bubbles transform into isolated stripes (not shown here).

Magnetization processes in $[(\mathrm{Co/Pt})_{X-1}/\mathrm{Co/Ir}]_4$ multilayers with X=15

Whereas the $[(\mathrm{Co/Pt})_{19}/\mathrm{Co/Ir}]_4$ multilayer shows the typical magnetization process and domain evolution described already in Chapter 4, by simply reducing the number of Co/Pt repeats, X, to 15, the magnetic behavior changes measurably. Figure 6.5 shows the magnetization curve of $[(\mathrm{Co/Pt})_{14}/\mathrm{Co/Ir}]_4$ multilayer as a function of a perpendicular oriented applied field. The magnetization increases continuously with field up to saturation (≈ 0.5 T). However, reducing the field, there are two discrete steps (marked by arrows) on the decreasing branch which suggests that the stacks are reversing independently at different external fields and the sample stays in a mixed state. These findings are supported also by the in-field MFM measurements presented in Fig. 6.6.

Figure 6.6 (a)-(d) displays the MFM images taken on the increasing branch of the hysteresis loop. In the zero field state (Fig. 6.6(a)), the sample displays a random maze domain pattern with a domain width of about 100 nm, i.e smaller than the 130 nm observed for the sample

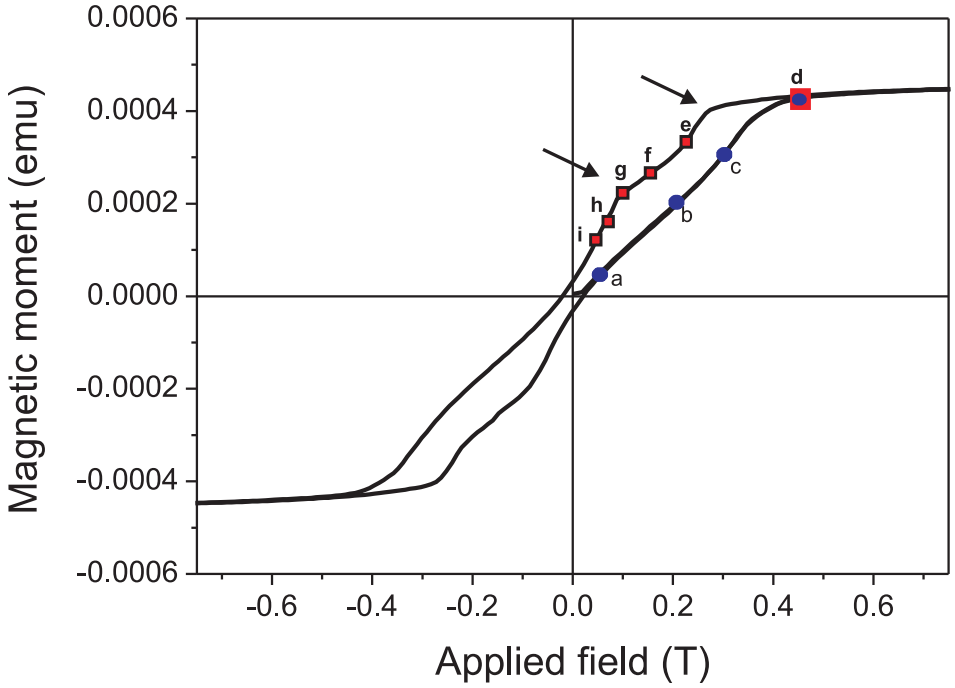

Fig. 6.5: Hysteresis loop measured by VSM with the field perpendicular to the sample surface. The points correspond to the field values applied in MFM measurements (Fig 6.6).

with X=20. This is in agreement with the theory that predicts a decrease of the domain width with decreasing film thickness (see Section 2.1.1, Fig. 2.3(b)). Towards saturation the domains aligned opposite to the applied field contract to form isolated stripe domains that contract further into bubble domains. Increasing the field further, the bubbles collapse at a critical field H_{bc} [Bra09] and the saturation is reached. The observed magnetization process resembles that observed in Co/Pt/Ru systems (Chapter 4 and 5).

After the sample was saturated, a series of MFM images was recorded on the decreasing branch of the hysteresis (Fig. 6.6 (d)-(i)). At 0.25 T, close to the first kink in the hysteresis, the first domains nucleate (Fig. 6.6(e)). The nucleated domains grow in length with decreasing field and expand through the whole sample very quickly. At this point the sample looks demagnetized although H>0. But when reducing the field further (at the 2nd kink in the hysteresis), new processes occur. Reversal domains with stronger contrast appear on the top of the already existing bright domains (Fig. 6.6(g)). With reducing field, the new domains expand (Fig 6.6(h)). Close to zero magnetic field they cover the entire area (Fig. 6.6(i)). Figure 6.7 (i)-(ii) presents the close-up images of Fig. 6.6 (g)-(h) where the newly nucleated domains grow along the length of the old bright domains (marked by the dashed blue line). This originates from a vertical extension of the existing nucleated band domains. These separate reversal steps might be explained by the sketch presented in Fig. 6.8. With

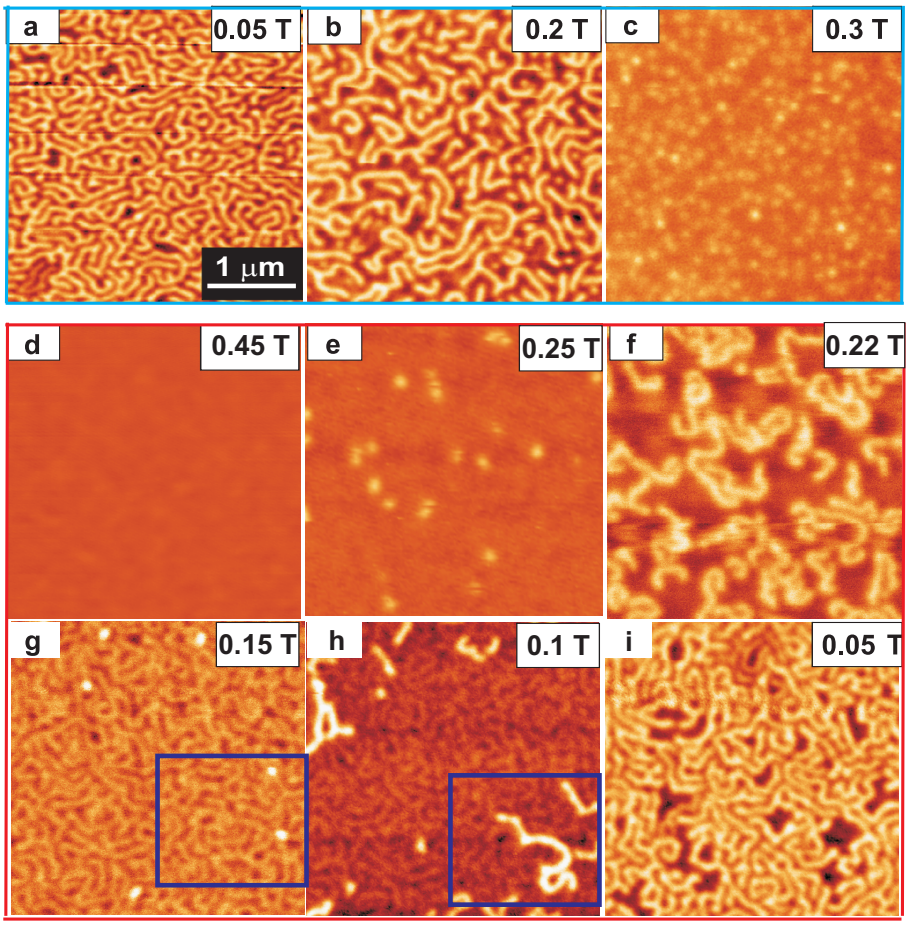

Fig. 6.6: Magnetic domain structures of $[(Co/Pt)_{X-1}/Co/Ir]_N$ multilayers with X=15 and N=4 measured by MFM in magnetic field. The marked area in (g) represents the zoomed area displayed in Fig 6.7.

decreasing field one of the center Co/Pt stacks is expected to reverse first because it is AF coupled on both sides and thus its exchange energy is twice as large as for the top or bottom stacks. This reversal is expected to happen simultaneously with the top stack at the nucleation field and then spread as a band domain through the whole area (Fig. 6.6 (e)-(g)). Here, the total energy has a minimum, considering the AF ground state of the system. After the first reversal is completed, decreasing the field further, the second reversal of the remaining stacks is happening. Judging from the enhanced magnetic contrast in the MFM image (Fig. 6.7(ii)) the bright domains expand vertically through the entire thickness of the sample and spread through the whole scanned area (Fig. 6.6(i)).

In summary, $[(\mathrm{Co}(0.4\ \mathrm{nm})/\mathrm{Pt}(0.7\ \mathrm{nm}))_{X-1}/\mathrm{Co}(0.4\ \mathrm{nm})/\mathrm{Ir}(0.5\ \mathrm{nm})]_4$ multilayers with perpendicular anisotropy show two different magnetization behaviors. For $[(\mathrm{Co/Pt})_{X-1}/\mathrm{Co/Ir}]_4$ with X=20 the reversal via vertical band domains through the whole film thickness is observed. The magnetization proceeds as typical for single layer thin films with perpendicular

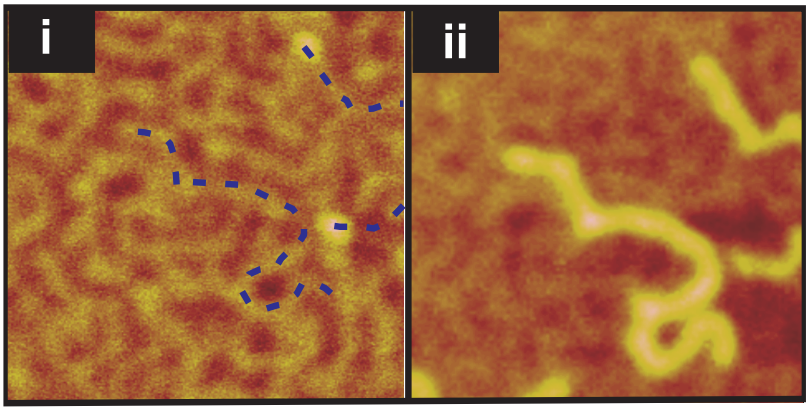

Fig. 6.7: Close-up images of Fig 6.6 (g-h), $(2.5\mu m)^2$ each, as indicated by the blue squares.

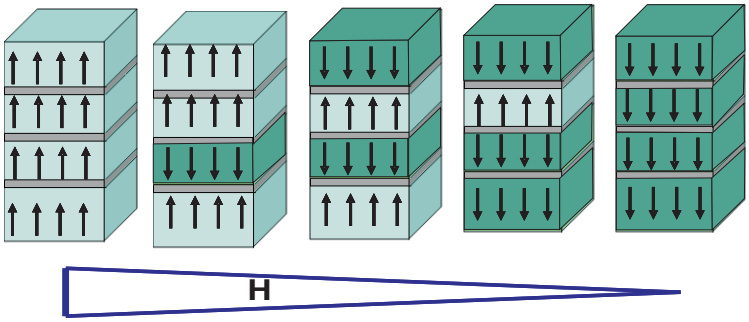

Fig. 6.8: Schematic presentation of the reversal mechanism observed in $[(\mathrm{Co/Pt})_{X-1}/\mathrm{Co/Ir}]_N$ multilayers with X=15 and N=4.

anisotropy via gradual growing of the domains oriented in the same direction as the applied field and contracting of those oriented opposite to the applied field into the bubble domain pattern, similar to (Co/Pt)/Ru multilayers (Chapter 4).

For X=15 the reversal occurs in two steps. First, two of the four stacks reverse simultaneously forming AF-coupled bands in the still magnetized matrix, which lead to a band domain structure with reduced contrast. In the second step, the last two stacks reverse, producing a vertical extension of the already nucleated AF band domains to form negatively magnetized FM bands. This is a new type of magnetization process which has not been considered before.

7 Co/Pd multilayers on nanospheres

Magnetic multilayers with perpendicular anisotropy are promising materials for the next generation of high density magnetic and magneto-optical recording media. To achieve high-density recording, the understanding of the magnetization reversal behavior is very important. A study of Co/Pd multilayers, deposited on arrays of nanospheres suitable for bit patterned media, will be presented in this chapter.

Since, in bit patterned media one magnetic nanodot corresponds to one recording bit, a deep understanding of the magnetization reversal in individual nanodots becomes very important. Many investigations on different shapes of structures such as squares, ellipses, and disks [Cow99, Shi00, Li01, Zhu02, Vaz03, Sor05] have been reported. In contrast to these nanostructures, a novel nanomaterial, which consists of a multilayer film on top of a spherical particle, was introduced recently [Alb05a]. Co/Pd multilayers are deposited on assemblies of nanospheres as is described in Chapter 3. The total thickness varies and so do the intrinsic magnetic properties, such as magnetic anisotropy, an important parameter which can affect the reversal process.
Co/Pd multilayers exhibit perpendicular magnetic anisotropy up to a Co layer thickness of a few monolayers where the interface anisotropy is large enough to overcome the shape anisotropy [Car85] (Chapter 2). Assuming an evaporation direction perpendicular to the substrate, the thickness of Co/Pd multilayers is highest at the top of the spheres and reduces towards the sides. The so-formed *nanocaps* on top of the spheres exhibit a radial symmetric anisotropy orientation across their surface (Fig. 7.1). Due to the small thickness of the individual Co layers (0.3 nm $\approx$ 1.5 monolayers), the ferromagnetic properties of the multilayers are suppressed at the intersections of the nanocaps, where the Co layer thickness reduces below 1 monolayer, forming a dilute Co-Pd alloy without significant anisotropy. This effect leads to an exchange isolation of magnetic nanocaps.

In the nanocap arrays, the magnetic exchange and magnetostatic interaction can be easily tuned by varying the particle diameter as well as the thickness of the deposited magnetic film [Ulb08]. At small a separation distance between the nanostructures, the dipole-dipole

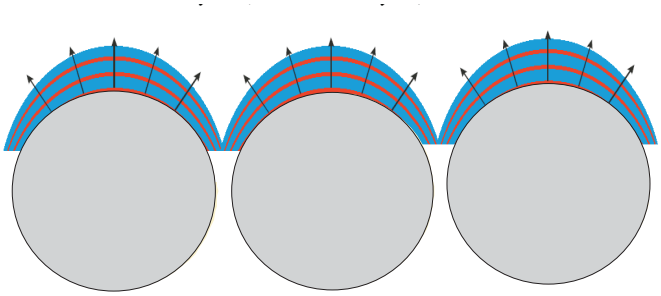

Fig. 7.1: Schematic pictures of the covered nanospheres [Alb05a].

interaction becomes rather important and will strongly influence the magnetization reversal in the array. Furthermore, a large film thickness in the range of the particle diameter may also result in direct exchange coupling of neighboring nanostructures. Consequently, a study of the magnetization reversal behavior of 58 nm particle arrays covered by $[Co/Pd]_N$ multilayer stacks exhibiting an out-of-plane easy axis of magnetization with varying bilayer number N will be presented.

7.1 MFM in field

In-field MFM measurements were performed to analyze locally the magnetic domain configuration of $[Co(0.3\ nm)/Pd(0.8\ nm)]_{80}$ nanocaps and to investigate their reversal behavior. Figure 7.2 shows a series of MFM images for different positive magnetic fields applied perpendicular to the sample during measurement, after the sample was previously magnetized in negative direction. The tip was magnetized in positive z-direction such that the dark and the bright contrasts correspond to domains with magnetization pointing “up” or “down”, respectively. At zero magnetic field (Fig. 7.2 (b)) a few isolated reversed nanocaps are observable (dark contrast, marked with white dots), which suggests that the nanocaps are in an isolated magnetic single domain state with the magnetization pointing “up” out of the film plane. The increase of the reverse magnetic field produces a successive switching of magnetic nanocaps. The spherical shape of the switched nanocaps suggests that each new “dark” domain corresponds to a single particle (Fig. 7.2 (c-f)) (circled with blue).
The discrepancies between the size of the particle and the size obtained by MFM measurements come from the MFM contrast which depends on the magnetic structure and the volume of the tip coating and is necessary broadened compared to the true size of the nanocap.
In addition to the single switching event, the reversal of entire regions consisting of several nanocaps is observed. The dominant individual switching of nanocaps with increasing field is seen as an indication for magnetic exchange decoupling in this sample.

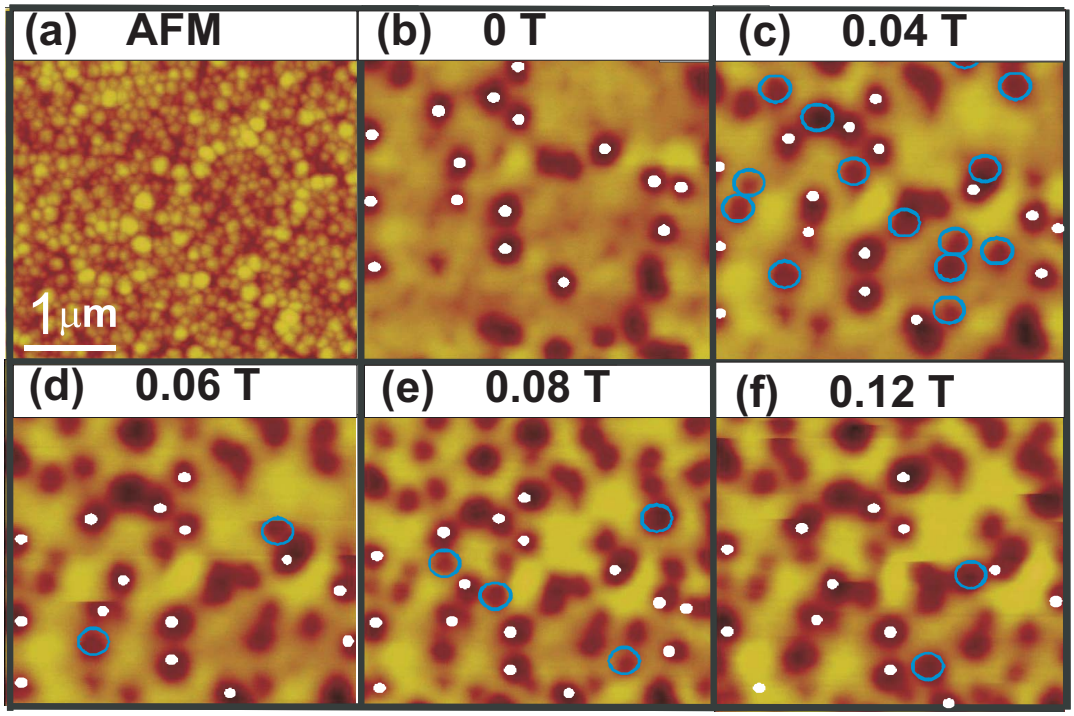

Fig. 7.2: Scanning probe microscopy observations on the Co/Pd multilayers on nanospheres (58 nm). Topological AFM image (a). MFM images after application of a perpendicular magnetic field of 0 T (b), 0.04 T (c), 0.06 T (d), 0.08 T (e), 0.12 T (f).

7.2 Magnetic Relaxation

The increase in magnetic recording density and consequently the reduction of particle sizes affects the magnetic stability in the media, which results in a time-dependent behavior known as magnetic relaxation. For zero applied magnetic field (H=0), a single domain particle with uniaxial anisotropy has two energetically equivalent ground states of opposite magnetization separated by an energy barrier ΔE_0 (Fig. 7.3). Applying a magnetic field, the height of the energy barrier is reduced and the magnetization is reversed [Née49]. If the applied field is parallel to the direction of the easy axis, the energy barrier can be expressed as:

$$\Delta E = K_u V \left(1 - \frac{H}{H_k}\right)^2 = \Delta E_0 \left(1 - \frac{H}{H_k}\right)^2 \tag{7.1}$$

where K_u is the anisotropy constant, V is the particle volume and $H_k = \frac{2K}{J_s}$, the anisotropy field. The time variation of magnetization of a particle when its magnetization reverses from positive saturation to negative saturation is expressed by:

$$M(t) = M_0 \left(2e^{\frac{-t}{\tau}} - 1\right) \tag{7.2}$$

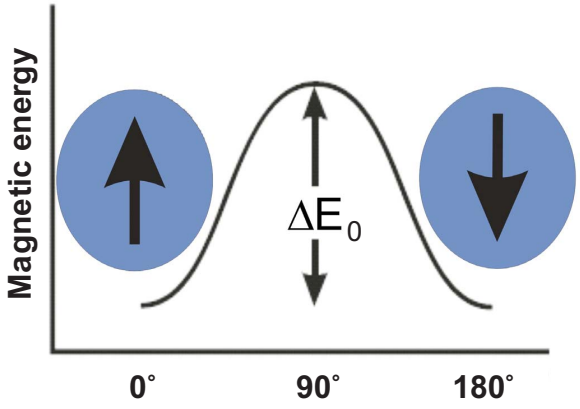

Fig. 7.3: Sketch of magnetic energy barrier vs magnetization angle

where $M_0 = J_0/\mu_0$ is the initial magnetization
τ is the relaxation time, given by the Néel-Arrhenius law:

$$\tau(\Delta E) = \tau_0 e^{\frac{\Delta E}{k_B T}} \tag{7.3}$$

k_B is the Boltzmann constant, T is the absolute temperature and $\Delta E = \Delta E(H)$ is the energy barrier in the presence of a constant field (Eq. 7.1).
Without a field, the stability factor $\frac{\Delta E_0}{k_B T}$ determines the time scale on which the stored information is stable. Requirements for recording media are $\beta = \frac{\Delta E_0}{k_B T} \approx 40 - 60$.

In a real system it is more likely that there are many particles with a corresponding energy barrier distribution, which leads to a modification of the magnetization relaxation:

$$M(t) = M_0 \int dE f(E) \left(2e^{\frac{-t}{\tau}} - 1\right) \tag{7.4}$$

where f(E) is the distribution function of energy barriers that have to be overcome by thermal fluctuations in order to change the equilibrium magnetization direction of the particles. Equation 7.4 is generally approximated by the well known logarithmic law [Str49]:

$$M(t) = const - S \ln t \tag{7.5}$$

where S is the magnetic viscosity.
The ratio of S/χ_{irr}, where χ_{irr} is the irreversible magnetic susceptibility, is defined as the fluctuation field H_f or in a more general form:

$$H_f = \frac{S(H,t)}{\chi_{irr}(H,t)} \tag{7.6}$$

The concept of the fluctuation field was first suggested by Néel [Née49] and was used to describe the effects of thermal activation on magnetization reversal. The idea of a fluctuation field led to the concept of an activation volume, which represents the volume of the magnetic moments within the material that switch together in the magnetization reversal, and is usually defined by:

$$V_{act} = \frac{k_B T}{J_s H_f} \tag{7.7}$$

Here, $k_B T$ is the thermal energy and J_s the saturation polarization.

Viscosity measurements for different Co/Pd thicknesses

Polar-Magneto Optical Kerr Effect (P-MOKE) hysteresis loops of $[Co/Pd]_N$ multilayers with different number of repeats are summarized in Fig. 7.4. The measurements were performed at

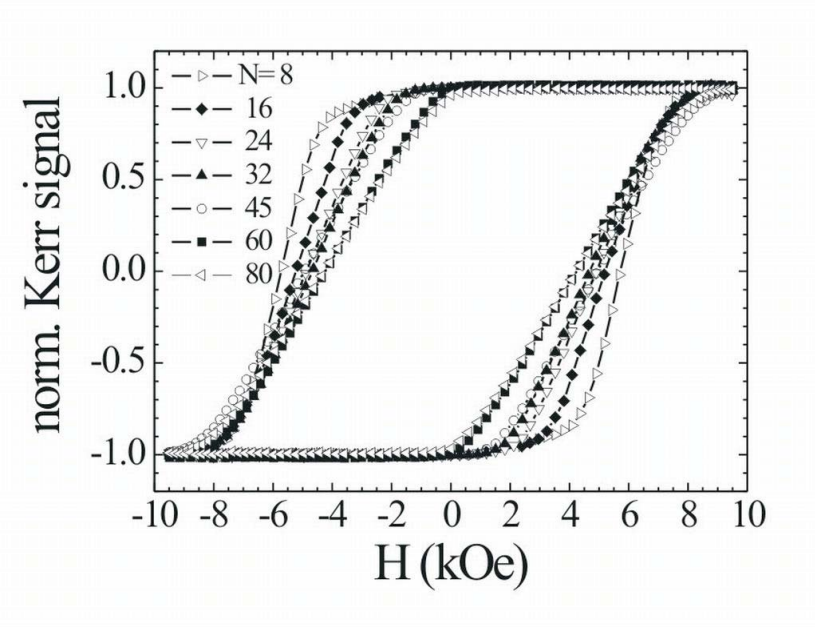

Fig. 7.4: Hysteresis loops of $(Co/Pd)_N$ multilayers with different numbers of repeats

the University of Konstanz by M. Albrecht and coworkers. Co/Pd multilayers on assemblies of particles reveal a systematic shearing of the hysteresis loop with increasing number of bilayers which is attributed to the effect of dipolar fields coming from the neighboring caps, which increase proportionally to the growing total magnetic moment of each nanocap [Hel07, Tho06]. In addition, with an increase of the bilayer number, the coercivity gradually decreases to a value of 0.45 T which might be related to the degradation of the interface quality for the thicker films. Additional information on the magnetization reversal can be obtained by mag-

netic viscosity measurements of $[Co/Pd]_N$ multilayers with different numbers of repeats (N), deposited on 58 nm spheres. For time dependent measurements the [Co(0.3 nm)/Pd(0.8 nm)]$_N$ multilayers with N = 16, 45 and 80, were first saturated at 3 T before applying different negative fields. At each applied reverse field, H, the magnetic moment was measured

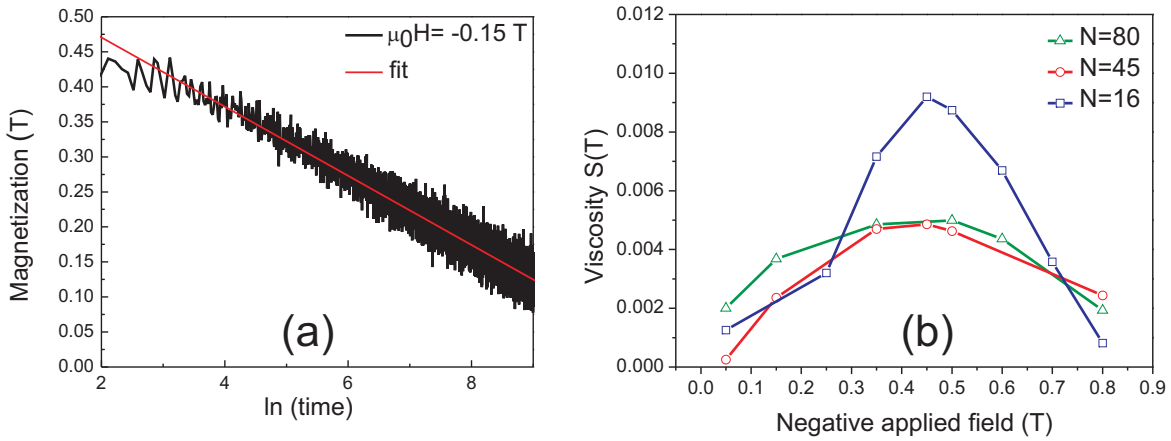

Fig. 7.5: (a) Magnetization relaxation data taken in the reverse field of 0.15 T for the $(Co/Pd)_N$ multilayer sample with N = 80. (b) The dependence of the magnetic viscosity, S on the negative applied field. The results were obtained for $(Co/Pd)_N$ multilayers with N=16, 45, 80.

for 9999 s. The magnetization relaxation follows a logarithmic time dependency over the entire range investigated (Fig. 7.5(a)), as expected for samples with a broad switching field distribution. The magnetic field dependence of the viscosity, S(H), was determined by fitting the measured M(t,H) curves according to Eq. (7.5) (Fig. 7.5(b)). The viscosity curves show a broad field dependence with a maximum close to the coercive field, where the energy barrier for magnetization reversal is near zero. With the decrease of the bilayer number to N = 16 the maximum of the magnetic viscosity drastically increases.

Recoil loops were measured by applying and removing a negative field (H_{appl}) to a magnetically saturated sample, and the negative field magnitude is increased successively (see insert in Fig. 7.6(a)). From these measurements the $M_r(H_{appl})$ curve was extracted (Fig. 7.6(a)). The irreversible susceptibility (χ_{irr}) was obtained by taking the derivative $\left(\frac{\partial M_r}{\partial H_{appl}}\right)$ of the remanent magnetization (M_r). The irreversible susceptibility, χ_{irr}(H), for the same set of samples is shown in Fig. 7.6(b). The data reveal a similar field dependence as observed in the viscosity measurements, with a pronounced peak around the coercive field. Furthermore, the maximum of the χ_{irr}(H) dependence scales in a similar way with the number of bilayers N, as found for the viscosity. Combining the magnetic viscosity and irreversible susceptibility

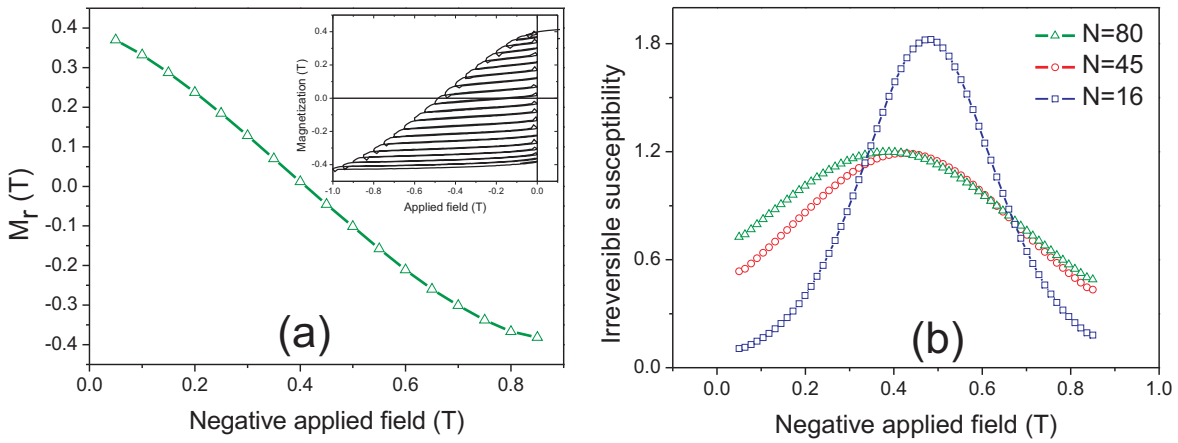

Fig. 7.6: (a) Remanent magnetization of a $[Co(0.3\ nm)/Pd(0.8\ nm)]_{80}$ sample as function of the applied field and recoil loops (insert). (b) Irreversible susceptibility as a function of the applied field for $(Co/Pd)_N$ multilayers with N=16, 45, 80.

measurements (Eq. 7.6), the magnetic field dependence of the fluctuation field, $H_f(H)$, is deduced. Although both, viscosity and irreversible susceptibility data reveal a strong magnetic field dependence, the fluctuation field is found to be almost independent of H as well as on the number of bilayers around the coercivity but tail off at lower and higher fields (Fig. 7.7, Table 7.1). The derived values $H_f(H_c; N)$ were used to extract the activation volume

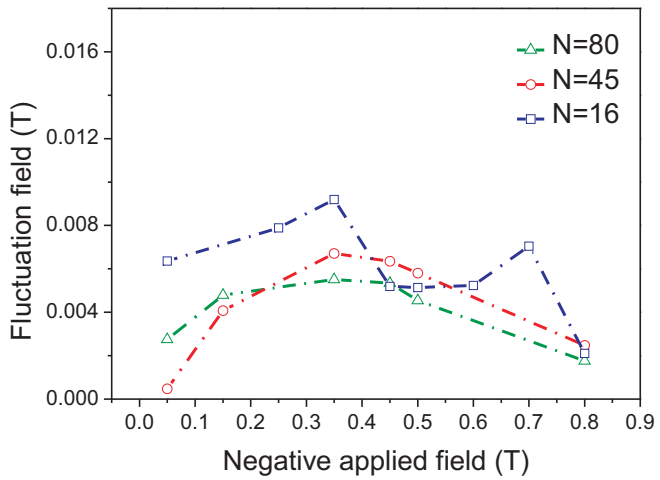

Fig. 7.7: Fluctuation field as a function of the applied field for $(Co/Pd)_N$ multilayers with N=16, 45, 80.

governing the reversal process (Eq. 7.7). With reducing the number of bilayers, N, the activation volume decreases slightly, but does not scale with the total film thickness (Table 7.1). It furthermore adopts a value of about 2000 nm^3, which is substantially smaller than the physical volume of an individual nanocap. The latter is in agreement with the observed

Tab. 7.1: Coercivity field (H_c), fluctuation field (H_f) at coercivity, activation volume (V_{act}) and stability factor ($\frac{\Delta E_0}{k_B T}$) for $(Co/Pd)_N$ multilayers with N = 80, 45, 16. The volume of an individual nanocap (V_{cap}) on the spherical particle is given for comparison.

Number of bilayers	$\mu_0 H_c$(mT)	$\mu_0 H_f$(mT)	$V_{act}(nm^3)$	$V_{cap}(nm^3)$	$\beta = \frac{\Delta E_0}{k_B T} \approx \frac{H_c}{H_f}$
N= 80	430	4.1	2.6 $\times 10^3$	590 $\times 10^3$	104
N= 45	500	5	2.3 $\times 10^3$	340 $\times 10^3$	100
N= 16	530	6	1.9 $\times 10^3$	120 $\times 10^3$	88

individual reversal of magnetic nanocaps (Fig. 7.2) indicating exchange decoupling between the neighboring nanocaps in the array. Moreover, the finding $V_{act} \ll V_{cap}$ further suggests an inhomogeneous magnetization reversal process rather than a coherent switching within the individual nanocaps for which $V_{act} \simeq V_{cap}$ is expected. This is in good agreement with the results of micromagnetic simulations [Ulb06], which suggest that a nucleation process starts in a circumferential ring around the nanocaps at about half the cap height, where the easy axis of magnetization adopts an angle of about 45° with respect to the substrate normal. In order to relate the estimated value of the activation volume to the physical volume relevant for the system under consideration, the angular modification of the magnetic parameters it has to be considered. According to the discussion above, the thickness of the individual layers changes with angle and results in a gradual transformation of the Co/Pd multilayers, which influences the magnetic anisotropy constant (K_U^0), the saturation magnetization (M_S^0), as well as the exchange parameter (A^0). The further estimation will be performed assuming the following angular dependence of the relevant magnetic parameters [Ulb06]:

$$K_U(\theta) = K_U^0 \times f(\theta);\ M_S(\theta) = M_S^0 \times f(\theta);\ A(\theta) = A^0 \times f(\theta)^2 \tag{7.8}$$

where $f(\theta) = exp[-(\theta - \theta_0)^2/\Delta^2]$ for $\theta > \theta_0$. Here Δ is the decay length and the angle, $\theta \simeq 45°$ is related to a certain critical thickness above which the degradation of magnetic properties of magnetic multilayers occurs. In this case, the width of the Bloch domain wall can be expressed as $d_B W(\theta) = d_0 \times f(\theta)$, where d_0 = 18 nm is the typical domain wall

width in Co/Pd multilayer films ($M_S^0 = 500$ emu/cm^3, $K_U^0 = 3 \times 10^5 erg/cm^3$, and $A_0 = 10^{-6}$ erg/cm). Assuming an isotropic nucleation process, the activation volume can be expressed as

$$V_{act} \approx d_{BW}(\theta)^3 \tag{7.9}$$

By comparing the measured activation volume with the one defined by Eq. (7.8) and Eq. (7.9), it is found that the nucleation event occurs at the position $\theta_N \approx \theta_0 + \delta \simeq 50°$, which corresponds to a δ of $\approx 5°$. This latter value is in good agreement with micromagnetic calculation for Co/Pd coated nanospheres, where the parameter δ is in the range of (2-5)° [Ulb06]. In total, the magnetization reversal in the nanocaps is interpreted as an isotropic nucleation process within the magnetic layer, which occurs on a length scale of the domain wall, additionally facilitated by the reduced anisotropy at the necks of the particle assembly.

The fluctuation field additionally allows to estimate the stability factor, β (Table 7.1), which is found to be higher than 80 even for the thinnest investigated magnetic film. This value is high enough to fulfill the thermal stability requirement for a recording media [Pir07].

Viscosity measurements for different temperatures

The hysteresis and the magnetization relaxation of $[Co(0.3\ nm)/Pd(0.8\ nm)]_{80}$ multilayers were measured at 100, 200, and 300 K, respectively. The hysteresis loops reveal increasing coercivity fields and magnetic moments with decreasing temperature (Fig. 7.8). The viscosity

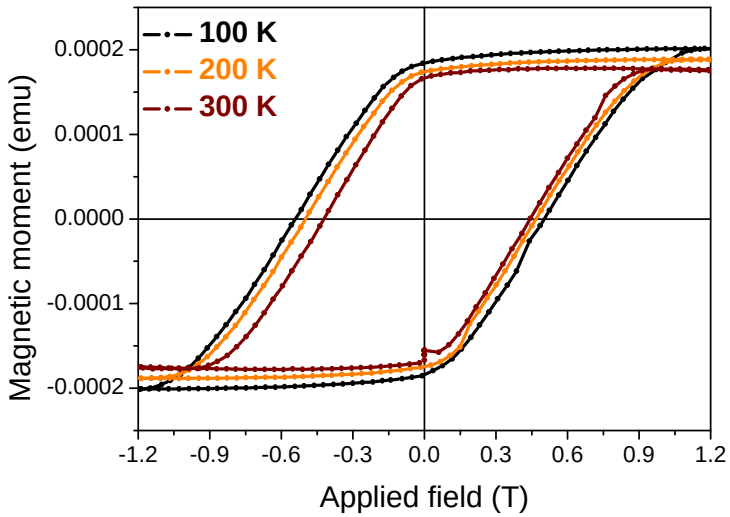

Fig. 7.8: Magnetization loops of $(Co/Pd)_{80}$ multilayers measured at 100, 200 and 300 K in out of plane magnetic field.

was measured as a function of field for all three temperatures by using the same experimental approach as described in the previous section. The S(H) curves for all three temperatures are displayed in Fig. 7.9(a).

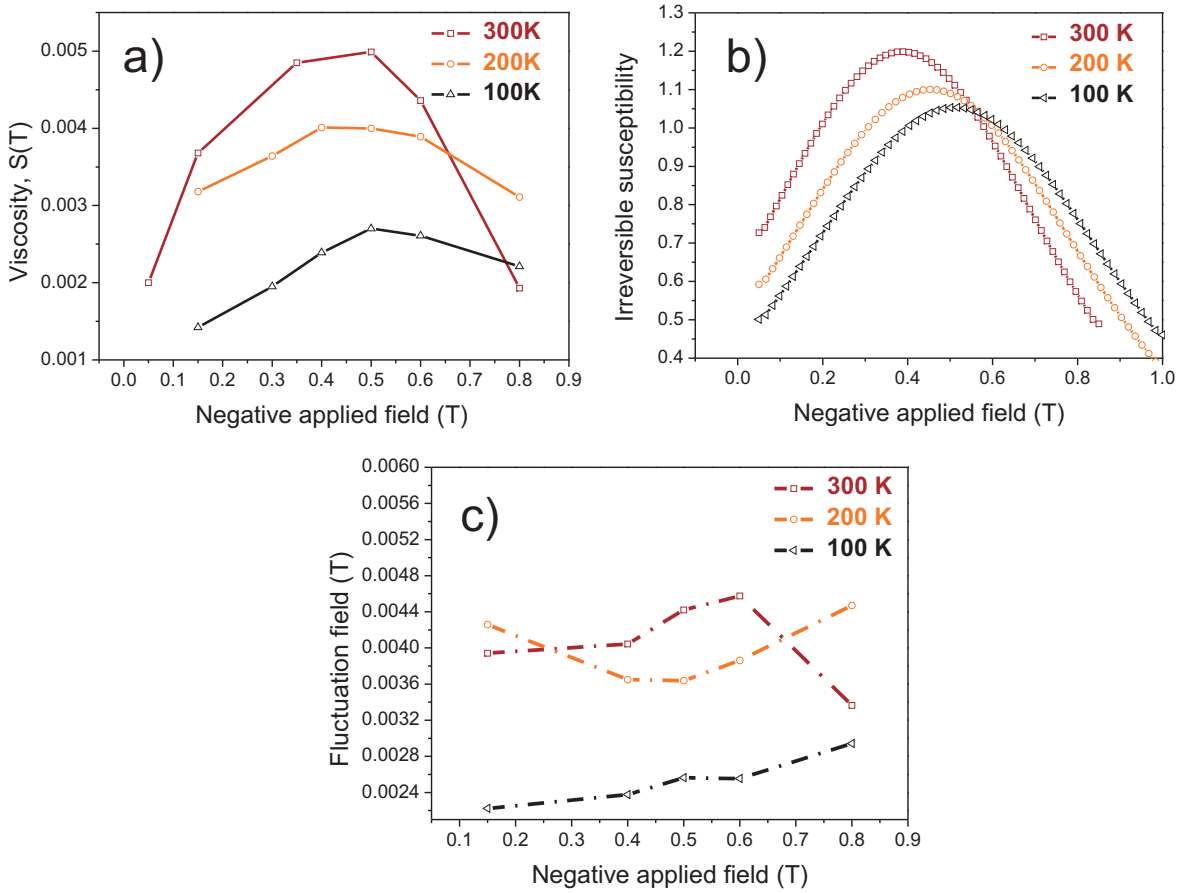

Fig. 7.9: Dependence on a negative applied field of (a) magnetic viscosity, S, (b) irreversible susceptibility, χ_{irr} and (c) fluctuation field, H_f. The results were obtained for $(Co/Pd)_{80}$ multilayers at 100 K, 200 K and 300 K.

The curves show a bell-shape and the maximum $S(H)$ was obtained at the coercivity field because of the minimum energy barrier. The same behavior is displayed also in Fig. 7.9(b) and 7.9(c) where with decreasing temperature the irreversible susceptibility and the fluctuation field decrease, proving that the reduced temperature minimizes the thermal instability in the sample. The calculations after Eq. (7.6) in the case of $(Co/Pd)_{80}$ show that the activation volumes decrease with temperature ($V_{act,300K}$= 2600 nm^3, $V_{act,200K}$= 2000 nm^3, $V_{act,100K}$= 1300 nm^3) while the stability factor, β, increases (β_{300K}= 104, β_{200K}= 130, β_{100K}= 200). The decrease of V_{act} with temperature was observed experimentally also in SmCo permanent

magnets [Pan02] and was predicted theoretically by Kirby el al. [Kir00]. It is in agreement with the isotropic nucleation model suggested in the previous section. With decreasing temperature the anisotropy constant K in Co/Pd multilayers increases and leads to the observed increase in coercivity, but it also reduces the domain wall width $d_{BW} = (A/K)^{1/2}$ and thus the activation volume according to Eq. (7.9).

Similar to the observations for multilayers prepared on flat substrates (Chapter 4, 5, 6), the Co/Pd multilayers deposited on assemblies of 58 nm particles reveal an interesting magnetization reversal behavior as function of thickness and temperature. The domain structure and switching events are now, however, largely localized due to the curved template. The coercive field and the switching field distribution are found to strongly depend on the thickness of the magnetic layer, indicating a strong influence of the magnetic dipole-dipole interaction on the magnetization reversal of the entire array of nanocaps. Moreover, magnetic viscosity measurements allowed the estimation of the magnetic activation volume representing the effect of thermal activation on the switching process. It was found that the magnetic activation volume is substantially smaller compared to the volume of the nanocap and almost independent of the number of bilayers supporting an inhomogeneous magnetization reversal process.

8 Conclusions and Outlook

In the present work a detailed study of the domain structure and the magnetization processes in AF-coupled Co/Pt multilayers and Co/Pd multilayers on arrays of 58 nm spheres has been presented. This is an unique attempt to understand nano-scale phase formation and corresponding ground state configuration in complex multilayers. The underlying mechanism of these complex systems is often found to depend upon the competition between different energy terms. Competing magnetic interactions produce higher-level patterns, mesoscopic order or formation of multiple phases with similar energies [Hel07]. The appearance of such mesoscopic order can be controlled by extrinsic parameters such as external magnetic field or temperature, while also depending on specific intrinsic parameters like film thickness and interaction between different layers or nanostructures.

Introducing AF exchange coupling to magnetic films with perpendicular anisotropy via nonmagnetic interlayers changes the energy balance that controls the band domain formation and reversal behavior for such systems, thus resulting in two competing reversal modes for the composite system. In the AF exchange dominated mode the magnetization is laterally correlated and vertically anti-correlated thus minimizing the interlayer exchange energy. In the dipolar dominated regime the magnetization is vertically correlated, but laterally anti-correlated in FM band domains that minimize the dipolar energy at the expense of the interlayer coupling. The different possible phases are described in Chapters 4 and 5.

The magnetization process of antiferromagnetically coupled $[(Co/Pt)_8/Co/Ru]_{18}$ multilayers with perpendicular anisotropy was investigated via magnetic force microscopy at room temperature by imaging the domain configuration in magnetic fields (Chapter 4).

In the zero-field state, due to the perpendicular anisotropy, band domains characteristic for ferromagnetic coupling are observed. By increasing the external magnetic field, the domain configuration first modifies gradually, then transforms from continuous into isolated stripes, and changes in the end into bubbles, which collapse at higher fields. Strip-out and collapse fields have been determined from domain imaging in narrow subsequent field steps.

A micromagnetic theory which treats stripe and bubble domains in multilayer films with small individual layer thicknesses has been applied to the experimentally studied multilayer architecture. The theoretical model can describe the equilibrium domain width of the sample in the ac-demagnetized state and the strip-out and collapse fields of the bubble domains with good precision.
In this study, the sample was structured into isolated square shaped elements with a lateral size of 12 μm using optical lithography. All observed domain structures are comparable to those of an extended film. For the given structure geometry and size we thus do not observe any influence of the lateral confinement on the domain configuration. For smaller structures this cannot be excluded and presents an interesting topic for future studies.

The magnetization reversal of perpendicular $[(Co/Pt)_7/Co/Ru]_{18}$ multilayers with AF ground state was investigated experimentally and theoretically in Chapter 5. In such a sample it was possible to alter the magnetic correlations from horizontal (AF state) to vertical (FM state) and vice versa via magnetic field cycling or temperature variation.
The magnetization reversal of AF-coupled multilayers has been investigated as a function of temperature in the range of 100-400 K. The AF-coupling gradually decreases with increasing temperature, before it abruptly vanishes at 400 K.
The domain evolution with magnetic field starting from the AF state was imaged by MFM in field. Applying small fields, the initial AF state is preserved. Beyond 0.2 T the AF state is overcome and ferromagnetic domains with magnetization pointing along the applied field are formed in the AF matrix. This corresponds to a simultaneous formation of surface and bulk metadomains, as predicted by the theory. Increasing the magnetic field further, the up-domains (metamagnetic domains) grow and expand across the whole area. This process, however, occurs first by an increase in length of the finite domain bands while their width stays essentially constant. At an applied magnetic field of about 0.38 T the metamagnetic up and down domains adopt an almost balanced configuration. Reducing the field again leads to the expected shrinking of the up-domains. At the lowest field, these isolated minority domains vanish almost completely, leaving the multilayer in the original homogeneous AF state. The direct observation of the metamagnetic domains confirms the theoretical description of this evolution.
In Chapter 4 the magnetization is dominated by ferromagnetic interaction where the reversal via vertical band domains through the whole film thickness is observed and well described by the theory. In Chapter 5 the AF coupling is very strong such that there is an homogeneous AF ground state at zero field. Here, the domain evolution is influenced by the AF coupling and confirms the theoretical prediction.

In Chapter 6 AF coupling is present in the Co/Pt/Ir system (X=15) but it is not so strong to lead to an homogeneous AF ground state. Ferromagnetic band domains are presented in the remanent state and AF coupling appears in an intermediate field state, forming a new type of domains which has not been considered so far. This proves how rich the possible phenomena are, depending on the balance between different energy scales. A new theoretical model to describe the new phase transition observed in the Co/Pt/Ir system could provide the necessary insight into a deeper understanding of coupling mechanism and magnetization reversal in these systems.

Contrary to the previous three chapters where the presented systems are globally planar with uniform properties, a multilayer deposition on a curved surface, where the topological change alters the film properties locally, has far reaching implications on the physics of nanoscale magnetism (Chapter 7). The magnetization reversal is driven by complex processes induced by the radial symmetric spatial variation of anisotropy orientations, which significantly alter the reversal process [Alb05a]. Co/Pd nanocaps reveal an interesting behavior as function of thickness and temperature. The coercive field and the switching field distribution are found to be strongly dependent on the thickness of the magnetic layer, indicating a strong influence of the magnetic dipole-dipole interaction on the magnetization reversal of the entire array of nanocaps. Moreover, magnetic viscosity measurements allowed the estimation of the magnetic activation volume representing the effect of thermal activation on the switching process. It was found that the magnetic activation volume is substantially smaller compared to the volume of the entire nanocap and almost independent of the number of bilayers supporting an inhomogeneous magnetization reversal process. The magnetization reversal in the nanocaps is interpreted as a nucleation process within the magnetic layer, which occurs in a length scale of the domain wall, additionally facilitated by the reduced anisotropy at the necks of the particle assembly.

List of Figures

List of Tables

Bibliography

[Alb05a] M. Albrecht, G. Hu, I. L. Guhr, T. C. Ulbrich, J. Boneberg, P. Leiderer and G. Schatz. Magnetic multilayers on nanospheres. *Nat. Mater.* **4**, 203 (2005)

[Alb05b] M. Albrecht, G. Hu, A. Moser, O. Hellwig and B. D. Terris. Magnetic dot arrays with multiple storage layers. *J. Appl. Phys.* **97**, 103910 (2005)

[Bai88] M. N. Baibich, J. M. Broto, A. Fert, F. N. Van Dau, F. Petroff, P. Etienne, G. Creuzet, A. Friederich and J. Chazelas. Giant Magnetoresistance of (001)Fe/(001)Cr Magnetic Superlattices. *Phys. Rev. Lett.* **61**, 2472 (1988)

[Bal07] V. Baltz, A. Marty, B. Rodmacq and B. Dieny. Magnetic domain replication in interacting bilayers with out-of-plane anisotropy: Application to Co/Pt multilayers. *Phys. Rev. B* **75**, 014406 (2007)

[Bar06a] A. Baruth, D. J. Keavney, J. D. Burton, K. Janicka, E. Y. Tsymbal, L. Yuan, S. H. Liou and S. Adenwalla. Origin of the interlayer exchange coupling in [Co/Pt]/NiO/[Co/Pt] multilayers studied with XAS, XMCD, and micromagnetic modeling. *Phys. Rev. B* **74**, 054419 (2006)

[Bar06b] A. Baruth, L. Yuan, J. D. Burton, K. Janicka, E. Y. Tsymbal, S. H. Liou and S. Adenwalla. Domain overlap in antiferromagnetically coupled [Co/Pt]/NiO/[Co/Pt] multilayers. *Appl. Phys. Lett.* **89**, 202505 (2006)

[Bla94] J. A. C. Bland and B. Heinrich. Ultrathin Magnetic Structures I. Springer (1994)

[Bob67] A. H. Bobeck. Properties and device applications of magnetic domains in orthoferrites. *Bell Syst. Tech. J.* **46**, 1901 (1967)

[Bra09] C. Bran, A. B. Butenko, N. S. Kiselev, U. Wolff, L. Schultz, O. Hellwig, U. K. Rossler, A. N. Bogdanov and V. Neu. Evolution of stripe and bubble domains in antiferromagnetically coupled $[(\mathrm{Co/Pt})_8/\mathrm{Co/Ru}]_{18}$ multilayers. *Phys. Rev. B* **79**, 024430 (2009)

[Bru88] P. Bruno. Dipolar magnetic surface anisotropy in ferromagnetic thin films with interfacial roughness. *J. Appl. Phys.* **64**, 3153 (1988)

[Bru91] P. Bruno and C. Chappert. Oscillatory coupling between ferromagnetic layers separated by a nonmagnetic metal spacer. *Phys. Rev. Lett.* **67**, 1602 (1991)

[Bru92] P. Bruno and C. Chappert. Ruderman-Kittel theory of oscillatory interlayer exchange coupling. *Phys. Rev. B* **46**, 261 (1992)

[Can87] C. L. Canedy, X. W. Li. and G. Xiao. Extraordinary Hall effect in (111) and (100)-orientated Co/Pt superlattices. *J. Appl. Phys.* **81**, 5367 (1987)

[Car85] P. S. Carcia, A. D. Meinhaldt and A Suna. Perpendicular magnetic anisotropy in Pd/Co thin film layered structures. *Appl. Phys. Lett.* **47**, 178 (1985)

[Car88] P. S. Carcia. Perpendicular magnetic anisotropy in Pd/Co and Pt/Co thin-film layered structures. *J. Appl. Phys.* **63**, 5066 (1988)

[Cha88] C. Chappert and P. Bruno. Magnetic anisotropy in metallic ultrathin films and related experiments on cobalt films. *J. Appl. Phys.* **64**, 5736 (1988)

[Cow99] R. P. Cowburn, D. K. Koltsov, A. O. Adeyeye, M. E. Welland and D. M. Tricker. Single-Domain Circular Nanomagnets. *Phys. Rev. Lett.* **83**, 1042 (1999)

[Dav04] J. E. Davies, O. Hellwig, E. E. Fullerton, G. Denbeaux, J. B. Kortright and K. Liu. Magnetization reversal of Co/Pt multilayers: Microscopic origin of high-field magnetic irreversibility. *Phys. Rev. B* **70**, 224434 (2004)

[dB88] F. J. A. den Broeder, D. Kuiper, A. P. van de Mosselaer and W. Hoving. Perpendicular Magnetic Anisotropy of Co-Au Multilayers Induced by Interface Sharpening. *Phys. Rev. Lett.* **60**, 2769 (1988)

[dB91] F. J. A. den Broeder, W. Hoving and P. J. H. Bloemen. Magnetic anisotropy of multilayers. *J. Magn. Magn. Mater.* **93**, 562 (1991)

[Din05] Y. Ding, J. H. Judy and J. P. Wang. Magnetoresistive sensors with perpendicular magnetic anisotropy. In *49th Annual Conference on Magnetism and Magnetic Materials*, Band 97 10N704. AIP (2005)

[Dra88] H. J. G. Draaisma, F. J. A. den Broeder and W. J. M. de Jonge. Perpendicular anisotropy in Pd/Co multilayers. *J. Appl. Phys.* **63**, 3479 (1988)

[Eim00] T. Eimuller, R. Kalchgruber, P. Fischer, G. Schutz, P. Guttmann, G. Schmahl, M. Kohler, K. Prugl, M. Scholz, F. Bammes and G. Bayreuther. Quantitative imaging of magnetization reversal in FeGd multilayers by magnetic transmission x-ray microscopy. *J. Appl. Phys.* **87**, 6478 (2000)

[Esc81] A.H. Eschenfelder. Magnetic Bubbles Technology. Springer (1981)

[Fer08] G. W. Fernando. Metallic multilayers and their applications. Elsevier (2008)

[FV02] J. Faure-Vincent, C. Tiusan, C. Bellouard, E. Popova, M. Hehn, F. Montaigne and A. Schuhl. Interlayer Magnetic Coupling Interactions of Two Ferromagnetic Layers by Spin Polarized Tunneling. *Phys. Rev. Lett.* **89**, 107206 (2002)

[Grü86] P. Grünberg, R. Schreiber, Y. Pang, M. B. Brodsky and H. Sowers. Layered Magnetic Structures: Evidence for Antiferromagnetic Coupling of Fe Layers across Cr Interlayers. *Phys. Rev. Lett.* **57**, 2442 (1986)

[Gra77] U. Gradmann. Magnetism of surfaces and interfaces. *J. Magn. Magn. Mater.* **6**, 173 (1977)

[Has89] S. Hashimoto, Y. Ochiai and K. Aso. Perpendicular Magnetic-Anisotropy and Magnetostriction of Sputtered Co/Pd and Co/Pt Multilayered Films. *J. Appl. Phys.* **66**, 4909 (1989)

[Hei94] B. Heinrich and J. A. C. Bland. Ultrathin Magnetic Structures II. Springer (1994)

[Hel03] O. Hellwig, T. L. Kirk, J. B. Kortright, A. Berger and E. E. Fullerton. A new phase diagram for layered antiferromagnetic films. *Nat. Mater.* **2**, 112 (2003)

[Hel07] O. Hellwig, A. Berger, J. B. Kortright and E. E. Fullerton. Domain structure and magnetization reversal of antiferromagnetically coupled perpendicular anisotropy films. *J. Magn. Magn. Mater.* **319**, 13 (2007)

[Hop05] H. Hopster and H. P. Oepen. Magnetic Microscopy of Nanostructures. Springer (2005)

[Hub98] A. Hubert and R. Schafer. Magnetic Domains. Springer (1998)

[Joh96] M. T. Johnson, P. J. H. Bloemen, F. J. A. Broeder and J. J. Vries. Magnetic anisotropy in metallic multilayers. *Reports on Progress in Physics* **59**, 1409 (1996)

[Khi06] S. Khizroev, Y. Hijazi, N. Amos, R. Chomko and D. Litvinov. Physics considerations in the design of three-dimensional and multilevel magnetic recording. *J. Appl. Phys.* **100**, 063907 (2006)

[Kir00] R. D. Kirby, M. Yu and D. J. Sellmyer. Activation volumes in thin film and particulate systems. In *J. Appl. Phys.*, Band 87 5696. AIP (2000)

[Kis07] N. S. Kiselev, I. E. Dragunov, U. K. Rossler and A. N. Bogdanov. Exchange shift of stripe domains in antiferromagnetically coupled multilayers. *Appl. Phys. Lett.* **91**, 132507 (2007)

[Kis08] N. S. Kiselev, U. K. Roessler, A. N. Bogdanov and O. Hellwig. Topological defects in antiferromagnetically coupled multilayers with perpendicular anisotropy. *Appl. Phys. Lett.* **93** (2008)

[Koo60] C. Kooy and U. Enz. Experimental and theoretical study of the domain configuration in thin layers of BaFe12O19. *Philips Res. Rep.* **15**, 7 (1960)

[Kyu96] K. Kyuno, J.-G. Ha, R. Yamamoto and S. Asano. Theoretical study on the Co layer thickness dependence of the magnetic anisotropy of Pd/Co multilayers. *Solid State Communications* **98**, 327 (1996)

[Lee90] C. H. Lee, R. F. C. Farrow, C. J. Lin, E. E. Marinero and C. J. Chien. Molecular-beam-epitaxial growth and magnetic properties of Co-Pt superlattices oriented along the [001], [110], and [111] axes of Pt. *Phys. Rev. B* **42**, 11384 (1990)

[Li01] S. P. Li, D. Peyrade, M. Natali, A. Lebib, Y. Chen, U. Ebels, L. D. Buda and K. Ounadjela. Flux Closure Structures in Cobalt Rings. *Phys. Rev. Lett.* **86**, 1102 (2001)

[Lin92] C. J. Lin and G.L.Gorman. Evaporated CoPt alloy films with strong perpendicular magnetic anisotropy. *Appl. Phys. Lett.* **61**, 1600 (1992)

[Liu03] Z. Y. Liu and S. Adenwalla. Oscillatory Interlayer Exchange Coupling and Its Temperature Dependence in [Pt/Co]3/NiO/[Co/Pt]3 Multilayers with Perpendicular Anisotropy. *Phys. Rev. Lett.* **91**, 037207 (2003)

[Liu04] Z. Y. Liu, L. Yue, D. J. Keavney and S. Adenwalla. Oscillatory interlayer exchange coupling in [Pt/Co] n /NiO/ [Co/Pt] n multilayers with perpendicular anisotropy: Dependence on NiO and Pt layer thicknesses. *Phys. Rev. B* **70**, 224423 (2004)

[Maj86] C. F. Majkrzak, J. W. Cable, J. Kwo, M. Hong, D. B. McWhan, Y. Yafet, J. V. Waszczak and C. Vettier. Observation of a Magnetic Antiphase Domain Structure with Long-Range Order in a Synthetic Gd-Y Superlattice. *Phys. Rev. Lett.* **56**, 2700 (1986)

[Man06] S. Mangin, D. Ravelosona, J. A. Katine, M. J. Carey, B. D. Terris and Eric E. Fullerton. Current-induced magnetization reversal in nanopillars with perpendicular anisotropy. *Nat. Mater.* **5**, 210 (2006)

[Mar87] Y. Martin and H. K. Wickramasinghe. Magnetic imaging by force microscopy with 1000 A resolution. *Appl. Phys. Lett.* **50**, 1455 (1987)

[Men06] H. Meng and J. P. Wang. Spin transfer in nanomagnetic devices with perpendicular anisotropy. *Appl. Phys. Lett.* **88**, 172506 (2006)

[Mor04] J. Moritz, F. Garcia, J. C. Toussaint, B. Dieny and J. P. Nozieres. Orange peel coupling in multilayers with perpendicular magnetic anisotropy: Application to (Co/Pt)-based exchange-biased spin-valves. *EPL (Europhysics Letters)* **65**, 123 (2004)

[Née49] L. Néel. Theorie du trainage magnetique des ferromagnetiques en grains fins avec applications aux terres cuites. *Ann. Geophys.* **5**, 99 (1949)

[Née54] L. Néel. L'approche á la saturation de la magnétostriction. *J. Phys. Radium* **15**, 376 (1954)

[Née62] L. Néel. Magnetisme - sur un nouveau mode de couplage entre les animantations de deux couches minces ferromagnetiques. *Comptes Rendus Hebdomadaires des Seances Acad.Sci.* **255**, 1676 (1962)

[Neu04] V. Neu, S. Melcher, U. Hannemann, S. Fahler and L. Schultz. Growth, microstructure, and magnetic properties of highly textured and highly coercive Nd-Fe-B films. *Phys. Rev. B* **70** (2004)

[Oun92] K. Ounadjela, D. Muller, A. Dinia, A. Arbaoui, P. Panissod and G. Suran. Perpendicular anisotropy and antiferromagnetic coupling in Co/Ru strained superlattices. *Phys. Rev. B* **45**, 7768 (1992)

[Pan02] I. Panagiotopoulos, M. Gjoka and D. Niarchos. Temperature dependence of the activation volume in high-temperature Sm(Co,Fe,Cu,Zr)[sub z] magnets. *J. Appl. Phys.* **92**, 7693 (2002)

[Par90] S. S. P. Parkin, N. More and K. P. Roche. Oscillations in exchange coupling and magnetoresistance in metallic superlattice structures: Co/Ru, Co/Cr, and Fe/Cr. *Phys. Rev. Lett.* **64**, 2304 (1990)

[Par91] S. S. P. Parkin. Systematic variation of the strength and oscillation period of indirect magnetic exchange coupling through the 3d, 4d, and 5d transition metals. *Phys. Rev. Lett.* **67**, 3598 (1991)

[PH92] M. Pardavi-Horvath, J. Oti, G. Vertesy, L. H. Bennett and L. J. Swartzendruber. A Preisach model study of demagnetized states. *J. Magn. Magn. Mater.* **104-107**, 313 (1992)

[Pir07] S. N. Piramanayagam. Perpendicular recording media for hard disk drives. *J. Appl. Phys.* **102**, 011301 (2007)

[Pop02] E. Popova, J. Faure-Vincent, C. Tiusan, C. Bellouard, H. Fischer, M. Hehn, F. Montaigne, M. Alnot, S. Andrieu, A. Schuhl, E. Snoeck and V. da Costa. Epitaxial MgO layer for low-resistance and coupling-free magnetic tunnel junctions. *Appl. Phys. Lett.* **81**, 1035 (2002)

[Por98] S. Porthun, L. Abelmann and C. Lodder. Magnetic force microscopy of thin film media for high density magnetic recording. *J. Magn. Magn. Mater.* **182**, 238 (1998)

[Rod06] B. Rodmacq, V. Baltz and B. Dieny. Macroscopic probing of domain configurations in interacting bilayers with perpendicular magnetic anisotropy. *Phys. Rev. B* **73**, 092405 (2006)

[Rud54] M. A. Ruderman and C. Kittel. Indirect Exchange Coupling of Nuclear Magnetic Moments by Conduction Electrons. *Phys. Rev.* **96**, 99 (1954)

[Rus01] A. W. Rushforth, P. C. Main, B. L. Gallagher, C. H. Marrows, B. J. Hickey, E. D. Dahlberg and P. Eames. Magnetic force microscopy studies of the domain structure of Co/Pd multilayers in a magnetic field. *J. Appl. Phys.* **89**, 7534 (2001)

[Sch99] I. K. Schuller, S. Kim and C. Leighton. Magnetic superlattices and multilayers. *J. Magn. Magn. Mater.* **200**, 571 (1999)

[She59] R. C. Sherwood, J. P. Remeika and H. J. Williams. Domain Behavior in Some Transparent Magnetic Oxides. *J. Appl. Phys.* **30**, 217 (1959)

[Shi00] T. Shinjo, T. Okuno, R. Hassdorf, K. Shigeto and T. Ono. Magnetic Vortex Core Observation in Circular Dots of Permalloy. *Science* **289**, 930 (2000)

[Sor05] J. Sort, A. Hoffmann, S. H. Chung, K. S. Buchanan, M. Grimsditch, M. D. Baro, B. Dieny and J. Nogues. Magnetization Reversal in Submicron Disks: Exchange Biased Vortices. *Phys. Rev. Lett.* **95**, 067201 (2005)

[Sti93] M. D. Stiles. Exchange coupling in magnetic heterostructures. *Phys. Rev. B* **48**, 7238 (1993)

[Str49] R. Street and J. C. Woolley. A Study of Magnetic Viscosity. *Proc. Phys. Soc.* **62**, 562 (1949)

[Str77] E. Stryjewski and N. Giordano. Metamagnetism. *Advances in Physics* **26**, 487 (1977)

[Ter05] B. D. Terris and T. Thomson. Nanofabricated and self-assembled magnetic structures as data storage media. *J. Phys. D-Appl. Phys.* **38**, R199 (2005)

[Thi69] A. A. Thiele. The theory of cylindrical magnetic domains. *Bell Syst. Tech. J.* **48**, 3287 (1969)

[Thi70] A. A. Thiele. Theory of Static Stability of Cylindrical Domains in Uniaxial Platelets. *J. Appl. Phys.* **41**, 1139 (1970)

[Tho06] T. Thomson, G. Hu and B. D. Terris. Intrinsic Distribution of Magnetic Anisotropy in Thin Films Probed by Patterned Nanostructures. *Phys. Rev. Lett.* **96**, 257204 (2006)

[Ulb06] T. C. Ulbrich, D. Makarov, G. Hu, I. L. Guhr, D. Suess, T. Schrefl and M. Albrecht. Magnetization Reversal in a Novel Gradient Nanomaterial. *Phys. Rev. Lett.* **96**, 077202 (2006)

[Ulb08] T. C. Ulbrich, D. Assmann and M. Albrecht. Magnetic properties of Co/Pt multilayers on self-assembled particle arrays. *J. Appl. Phys.* **104**, 084311 (2008)

[Ung91] J. Unguris, R. J. Celotta and D. T. Pierce. Observation of two different oscillation periods in the exchange coupling of Fe/Cr/Fe(100). *Phys. Rev. Lett.* **67**, 140 (1991)

[Vaz03] C. A. F. Vaz, L. Lopez-Diaz, M. Kläui, J. A. C. Bland, T. L. Monchesky, J. Unguris and Z. Cui. Direct observation of remanent magnetic states in epitaxial fcc Co small disks. *Phys. Rev. B* **67**, 140405 (2003)

[Yos57] K. Yosida. Magnetic Properties of Cu-Mn Alloys. *Phys. Rev.* **106**, 893 (1957)

[Zep89] W. B. Zeper, F.J.A.M. Greidanus, P.F. Carcia and C.R. Fincher. Perpendicular magnetic anisotropy and magneto-optical Kerr effect of vapor-deposited Co/Pt-layered structures. *J. Appl. Phys.* **65**, 4971 (1989)

[Zhu02] X. Zhu, P. Grütter, V. Metlushko and B. Ilic. Magnetic force microscopy study of electron-beam-patterned soft permalloy particles: Technique and magnetization behavior. *Phys. Rev. B* **66**, 024423 (2002)